

Flux density measurements of a complete sample of faint blazars

F. Mantovani, M. Bondi, and K.-H. Mack

Istituto di Radioastronomia – INAF, via Gobetti 101, I-40129 Bologna, Italy

Received August 28, 2018; accepted ???

ABSTRACT

Aims. We performed observations with the Effelsberg 100-m radio telescope to measure flux densities and polarised emission of sources selected from the “Deep X-ray Radio Blazar Survey” (DXRBS) to better define their spectral index behaviour in the radio band, with the aim to construct a homogeneous sample of blazars.

Methods. Sources were observed at four different frequencies with the Effelsberg 100-m telescope. We complemented these measurements with flux density data at 1.4 GHz derived from the NRAO VLA Sky Survey (NVSS).

Results. The spectral indices of a sample of faint blazars were computed making use of almost simultaneous measurements. Sixty-six percent of the sources can be classified as “bona fide” blazars. Seven objects show a clearly inverted spectral index. Seventeen sources previously classified as flat spectrum radio quasars (FSRQ) are actually steep spectrum radio quasars (SSRQ). The flux densities obtained with the Effelsberg 100-m telescope at 5 GHz are compared with the flux densities listed in the Green Bank (GB6) survey and in the Parkes-MIT-NRAO (PMN) catalogue. About 43% of the sources in our sample exhibit flux density variations on temporal scales of 19 or 22 years.

Conclusions. We confirm that 75 out of 103 sources of the DXRBS are indeed FSRQs. Twenty-seven sources show a spectral index steeper than -0.5 and should be classified as SSRQs. Polarised emission was detected for 36 sources at 4.85 GHz. The median value of the percentage of polarised emission is $(5.8 \pm 0.9)\%$. Five sources show rotation measure (RM) values $> 200 \text{ rad m}^{-2}$.

Key words. flux density, spectral index, polarisation – galaxies: quasars: BL Lacs: radio continuum: galaxies

1. Introduction

Blazars are an extreme class of active galactic nuclei (AGN) characterized by high luminosity, rapid variability, and high polarisation. In the radio band, blazars are core-dominated objects with apparent superluminal speeds along relativistic jets pointed close to the observer’s line of sight. Blazars have flat spectral indices and include FSRQs and BL Lacertae objects, the counterparts of high- and low-luminosity radio galaxies. Owing to their orientation with respect to the line of sight, blazars represent less than 5% of all AGN, a quite rare class of sources.

The first blazar samples were selected at relatively high limiting flux densities in the radio or X-ray band, $\sim 1 \text{ Jy}$ or a few times $10^{-13} \text{ ergs cm}^{-2} \text{ s}^{-1}$, respectively (Stickel et al. 1991; Wood et al. 1984; Kollgaard et al. 1996; Gioia et al. 1990; Stocke et al. 1991; Perlman et al. 1996).

In the last decade of the past century, many efforts have been made to select samples of blazars that could be representative of the whole population (Marchã 1994; Laurent-Muehleisen et al. 1999; Caccianiga et al. 1999; Bondi et al. 2001). A deeper, more comprehensive sample of blazars has been constructed by Perlman et al. (1998) and by Landt et al. (2001): the “Deep X-ray Radio Blazar Survey” (DXRBS). The DXRBS has been constructed by cross-correlating all ROSAT sources of the WGCAT catalogue (White, Giommi & Angelini 1995) and radio sources with flat radio spectra. The radio flux densities have been taken from available catalogues, like the Green Bank GB6 (Gregory et al. 1996), NORTH20CM (White & Becker 1992), and Parkes-MIT-NRAO PMN (Griffith & Wright 1993).

The DXRBS sample is currently the faintest, down to $\sim 50 \text{ mJy}$ at 5 GHz and power $\sim 10^{24} \text{ W Hz}^{-1}$, and most extensive blazar sample with nearly complete optical spectroscopic identifications. The radio spectral information of the DXRBS sources is based on non-simultaneous measurements at just two frequencies. Simultaneous flux density measurements at several frequencies are needed to obtain more reliable spectral indices.

In this paper we present the results from the simultaneous multi-frequency campaign made with the Effelsberg 100-m telescope. In Section 2 we summarise the observations and data processing. In Section 3 we present results from the observations. Conclusions are presented in sections 4 and 5.

2. Observations and data reduction

The sample of faint blazars, subject of the present investigation, was constructed from the DXRBS catalogue. We selected all sources with $\text{Dec} \geq -20^\circ$ and obtained a sample of 103 blazars, 74 of which were originally classified as FSRQs, 17 as SSRQs, and 12 as BL Lac objects. They represent a complete sample of objects with known optical spectroscopic identifications. Redshifts are available for 99 out of 103 sources.

We have made simultaneous flux density measurements with the Effelsberg 100-m telescope at 2.64 GHz, 4.85 GHz, 8.35 GHz, and/or 10.45 GHz of the full sample of 103 sources.

The observations were carried out in the period 1–6 July 2009. All sources in the sample are point-like to the Effelsberg telescope beams. They are also bright enough to be observed by cross-scanning along the azimuth and elevation axes, with four to eight subscans to determine the total intensity and polarisation characteristics.

Send offprint requests to: Franco Mantovani
e-mail: fmantovani@ira.inaf.it

Details about the observation mode, calibration and evaluation of flux density and polarised emission errors can be found in Mantovani et al. (2009).

2.1. Source coordinates and flux density measurements

The positions for the sources listed in the DXRBS catalogue are taken from the GB6 survey for $0^\circ < \text{Dec.} < 70^\circ$ or PMN surveys for $-20^\circ < \text{Dec.} < 0^\circ$. To improve the positional accuracy even more, we have derived the positions of the DXRBS objects from the FIRST survey (Becker et al. 1994) and from the NVSS (Condon et al. 1998) at 1.4 GHz. Images of a $15' \times 15'$ field centred at the GB6 or PMN positions were extracted from the two surveys, and new coordinates were obtained using the AIPS task JMFIT. Positions for 63 DXRBS objects were obtained from the FIRST catalogue. For the remaining sources the coordinates were from the NVSS. The new coordinates are reported in Table 1 together with flux density measurements at 1.4 GHz from the NVSS and our own flux density measurements with the Effelsberg 100-m telescope. The source 3C 286 was observed as flux density and polarisation calibrator. The flux density measurements at all available frequencies are on the Baars et al. (1977) scale.

3. Results

Originally the spectral indices in DXRBS were defined from flux density measurements at 1.4 GHz and 5 GHz from the existing catalogues. This approach, however, causes a major problem. Blazars are variable sources at all bands of the electromagnetic spectrum. Measurements at different frequencies obtained at different epochs may cause a misleading classification of the spectral indices. Consequently, we performed accurate flux density measurements of the DXRBS sample at several of the frequencies available at the Effelsberg 100-m telescope.

3.1. Spectral index behaviour

Single-epoch spectral indices are determined making use of flux density measurements taken at 2.64 GHz, 4.85 GHz, 8.35 GHz, and/or 10.45 GHz. Flux densities at 1.4 GHz were taken from the NVSS. We make the assumption that sources alter very little in flux density with time at frequencies lower than about 2 GHz (Padielli et al. 1987). The spectral indices (α averaged over the whole spectra), have been classified as follows:

- a) “steep” spectral index when $\alpha \leq -0.5$; “steep +” for $\alpha < -0.7$;
- b) “flat” spectral index when $\alpha > -0.5$;
- c) “steep–flat” spectral index when α is steep at lower frequencies and flattens at higher frequencies;
- d) “flat–steep” spectral index when α is flat at lower frequencies and steep at higher frequencies;
- e) a giga-Hertz peaked (“GPS”) spectral index when the shape is convex with a peak at about the intermediate observing frequencies;
- f) “inverted” spectrum when the spectral index shape is mainly straight and the flux density clearly increases with frequency.

Examples of spectral index plots are shown in Fig. 1. The full set of spectral index plots is presented in Appendix A. A crude classification of the spectral index behaviour is summarized in Table 2.

The spectral index type is listed in Table 3. The α values between subsequent frequencies can be found in the spectral index plots in Appendix A. For the source J0513.8+0156 only one flux density measurement is available due to technical problems during the observations.

3.2. Flux density variability

Observations made at 4.85 GHz have also allowed us to look for any flux density variability through a comparison with the measurements available in the GB6 and PMN catalogues.

The GB6 survey has been built from observations performed in 1986–87. The catalogue contains sources with $S_{4.85 \text{ GHz}} > 18 \text{ mJy}$. A 20 mJy source has a typical error of 4–5 mJy. The PMN survey was conducted in 1990 using the Parkes 64-m radiotelescope and the NRAO seven-beam receiver at 4.85 GHz covering the whole sky in the declination range $-87^\circ < \delta < 10^\circ$. The PMN survey in its equatorial region, which is the one relevant for the comparison with our southern sources, has a flux density limit of 40 mJy. The sources in our sample observed by Effelsberg at 4.85 GHz and listed in the GB6 and PMN catalogues are 67 and 35, respectively. Effelsberg measurements are reported in Table 1, while GB6 and PMN measurements are listed in Table 3.

Firstly, we checked for any possible systematic difference between our measurements and those from the GB6 and PMN catalogues. In Fig. 3 we plot the Effelsberg flux densities *versus* the GB6 (points) or PMN (triangle) flux densities at 5 GHz. The flux density measurements are well-placed around the equal flux density line, with a scatter given by the variability. More quantitatively, the mean value and dispersion for the ratio between the Effelsberg and GB6 flux densities are 1.00 and 0.07. From the comparison between the Effelsberg and the PMN flux density we obtain a slightly lower value with a much higher dispersion 0.97 and 0.54, respectively. This is consistent with the original finding from the comparison between the PMN and GB6 surveys.

For the sources in the GB6 catalogue we can compare observations made at three epochs: our data taken in 2009 and the two measurements made in 1986 and 1987, which were used for the GB6 catalogue. We used the JAVA applet available at the GB6 catalogue web page (<http://pulsar.phas.ubc.ca/>) to retrieve the flux densities at epochs 1986 and 1987 for all our sources with declination $> 0^\circ$.

The long-term variability in the GB6 catalogue is parametrized using the following quantity:

$$R = |S_{87} - S_{86}| / \sigma ,$$

where σ is the combined error of the two flux density measurements. Out of the 67 sources in common, four do not possess a calculated R value because they lack either the 1986 or 1987 flux density measurement. We calculated the same quantity R using our 2009 Effelsberg observations and the 1987 measurements from the GB6 survey and we plot the outcome in Fig. 4. We consider variables the sources with $R > 2$. We find that 55% of the sources (35 objects) do not show significant variations both in the time intervals 1986 to 1987 and 1987 to 2009, 11% of the sources (seven objects) were found variable between 1986–1987 compared to 40% (twentyfive objects) of variable sources between 1987 and 2009; finally 5% of the sources (three objects) showed significant variability between 1986 and 1987 but were found non-variable on the longer time 1987–2009. Considering also the four objects for which we do not have the R_{86-87} values,

we have a total of 28 radio sources (42%) with $R_{87-09} > 2$ and therefore, according to the threshold adopted, variable in a time interval of 22 years.

We calculated R also for the 35 sources with $\delta \leq 0$ that have the PMN measurements and we find that 45% of the sources (16 objects) have $R_{90-09} > 2$. This fraction is consistent with that of the northern sources and we can conclude that 43% of the DXBRS sample presented in this paper show significant variability on a time interval of about 20 years. The quantity R is reported in Table 3.

3.3. Polarised emission

The Effelsberg observations were carried out in full polarisation. We consider a source to be polarised when the intensity of the polarised emission is three times the rms error estimated for the polarised emission source by source. Results are presented in Table 4.

At 1.4 GHz, 27 sources show a polarised emission below the detection limits according to the data extracted from the NVSS. One source in our list was not found by the extraction process. The remaining sources have a median value of the fractional polarisation m of $3.0^{+0.4}_{-0.8}\%$.

At 2.64 GHz we found 25 sources polarised with a median value of m of $4.9^{+1.1}_{-0.4}\%$. At 4.85 GHz we found 36 sources polarised with a median m of $(5.8 \pm 0.9)\%$. These integrated values are considered typical of AGN. They can be compared with those achieved by Mantovani et al. (2009) on a sample of compact steep-spectrum sources and by Klein et al. (2003) on a sample of steep spectrum extended radio sources selected from the B3-VLA sample, as shown in Table 5. The trend is a quick decrease in the fractional polarisation with increasing wavelength. However, cases of repolarisation, i.e. an increase of fractional polarisation towards longer wavelengths, were reported, like that for the source 3C455 (see Mantovani et al. (2009), worth of further investigation. Repolarisation is seen for thirteen faint blazars in our sample, which show a peak of m at about 2.6 GHz. Systematic instrumental effects to possibly explain this behaviour can be excluded. More accurate observations are required to confirm this trend of the fractional polarisation.

Rotation measure could be calculated for 27 sources, of which seventeen are classified as *bonafide* blazars (FSRQs), nine as SSRQs, and one as a GPS object, according to our flux density measurements. The RM values are in the range from 0 to 1950 rad m^{-2} in the source rest frame (i.e. RM redshift corrected). The majority of the sources show a quite low RM. No clear correlation of m with the spectral index type (SSRQs or FSRQs) could be found. An example of RM and m plot is presented in Fig. 2. The full set of plots can be found in Appendix B.

4. Comments on individual sources

There are a few sources worth of brief comments.

J0204.8+1514 – Adding 180° to the EVPA at 1.4 GHz produces just a slightly worse fit. In this case the RM is -22.5 rad m^{-2} .

J1025.9+1253 – A fit of equal goodness and a RM of -85.5 rad m^{-2} results from rotation of the EVPA at 2.64 GHz by 180° and the EVPA at 1.4 GHz by 360° .

J0937.1+5008 – The source J0937.1+5008 exhibits a high degree of variability at 5 GHz, of the order of 60% to 70% on a time scale of about 22 years comparing the Effelsberg flux density

and the GB6 flux density. Moreover, it shows an increase in flux density by a factor of 2.3 comparing the Effelsberg flux density with the flux density measured few months later (22 Oct 2009) with the European VLBI Network observations at the same frequency (Mantovani et al. in prep.). Short-term variability was not found comparing the two measurements made in 1986 and 1987 by the GB6. A preliminary milli-arcsecond resolution image of J0937.1+5008 (resolution better than 5 mas; rms noise 1.5 mJy/beam) shows that the source is point-like (Mantovani et al. 2010). J0937.1+5008 was detected by the Fermi Gamma-Ray Space Telescope (Abdo et al. 2010). This source presents a peculiar “concave” spectral index as shown in Fig. 5. A similar spectral index shape is also shown by the source J1028.6–0336.

J1626.6+5809 – Removing the EVPA at 1.4 GHz, a good fit is achieved using the three Effelsberg measurements and a rotation by 180° at 2.64 GHz. The RM in this case is -16.4 rad m^{-2} .

J1648.4+4104 – A better fit to the data can be achieved by rotating the EVPA at 1.4 GHz by 360° . The RM is now 170 rad m^{-2} .

5. Conclusions

Our investigation aims at verifying the spectral index classification of the DXRBS sample. We define a spectral index $\alpha \leq -0.5$ as “steep”. If $\alpha > -0.5$ it is considered “flat”. However, the spectra often show a complex shape, i.e. not a steep or flat straight line. This makes the classification more difficult. We have attempted a “crude” classification source by source in Table 3, while spectral indices are available in the plots we produced for each source (see Appendix A).

The majority of sources, 66 out of 102 (for one source we do not have enough measurements) can be considered *bonafide* blazars, namely those with “flat”, “steep-flat”, “inverted”, and possibly also “flat-steep” spectra in the present classification.

Several sources changed their spectral index classification with respect to that reported in the original list by Perlman et al. (1998) and by Landt et al. (2001). Among them we have nine sources with a “convex” spectral index peaking in the GHz regime, which should be more properly defined as giga-Hertz peaked sources (GPS). These sources cannot be considered blazars. We found that 17 sources previously classified as FSRQs are actually SSRQs. Moreover, we found six sources with spectral indices even steeper than -0.7 , failing one of the original selection criteria. In total, we found that 27 sources can be classified as SSRQs showing a spectral index < -0.5 . This result suggests that a statistically meaningful comparison between FSRQs and SSRQs in the same flux density limited complete sample is possible.

We can anticipate that all 42 sources belonging to our sample observed so far with the EVN at 5 GHz have been detected (Mantovani et al., in prep.). Six sources, previously classified SSRQs (and found with $\alpha < -0.7$), host AGN. Two of them show a core-jet structure, while the remaining four are point-like at a resolution better than 5 milli-arcseconds. The EVN to Effelsberg flux density ratio ranges from 0.05 to 0.8. Most of their radio emission is therefore not coming from the cores of these sources.

Fourty-three percent of the DXRBS sample show significant variability on a time scale of 19–22 years; 11% show short-term variability comparing Green Bank flux density measurements taken one year apart in 1986 and 1987.

About 25% of the sources show polarised emission above the detection limits of our observations. We also extracted polarimetric information from the NVSS to collect at least the

three measurements needed to compute the RM diminishing the $n\pi$ ambiguity. The majority of the sources show $|\text{RM}| < 200 \text{ rad m}^{-2}$ in the source rest frame, possibly produced by the Faraday depth of the Galactic foreground. In nine cases, namely J0029.0+0509, J0322.6–1335, J0434.3–1443, J0510.0+1800, J0518.2+0624, J0744.8+2920, J1400.7+0425, J1419.1+0603, and J1648.4+4104 the rest frame RM are in the range of $200 < |\text{RM}| < 1940 \text{ rad m}^{-2}$. The highest value found is $1938.8 \text{ rad m}^{-2}$ for the source J0434.3–1443.

Acknowledgements. We thank an anonymous referee for his/her very helpful comments and suggestions, and for a careful reading of the manuscript of this paper. This work is based on observations with the 100-m telescope of the MPIfR (Max-Planck-Institut für Radioastronomie) at Effelsberg. It has benefited from research funding from the European Community's Framework Programme under RadioNet R113CT 2003 5058187. FM likes to thank Anton Zensus for the kind hospitality at the Max-Planck-Institut für Radioastronomie, Bonn, for a period during which part of this work has been done. The authors like to thank Heinz Andernach for suggesting to check for short-term flux density variability making use of Green Bank measurements. This research has made use of the NASA/IPAC Extragalactic Database (NED), which is operated by the Jet Propulsion Laboratory, California Institute of Technology, under contract with the National Aeronautics and Space Administration. Part of this work was supported by the: COST Action MP0905 'Black Holes in a Violent Universe'.

References

- Abdo, A.A., Ackermann, M., Ajello, M. et al. 2010, *ApJS*, 188, 405
 Baars, J.W.M., Genzel, R., Pauliny-Toth, I.I.K. & Witzel, A. 1977, *A&A*, 61, 99
 Becker et al. 1994, *ASP Conference Series*, v. 61, eds. Crabtree, Hanisch & Barnes, p. 165
 Bondi, M., Marchã, M., Dallacasa, D., Stanghellini, C. 2001, *MNRAS*, 325, 1109
 Caccianiga, A., Maccacaro, T., Wolter, A. et al. 1999, *ApJ*, 513, 51
 Condon, J.J., Cotton, W.D., Greisen, E.W. et al. 1998, *AJ*, 115, 1693
 Gioia, I.M., Maccacaro, T., Schild, R.E. et al. 1990, *ApJS*, 72, 567
 Gregory, P.C., Scott, W.K., Douglas, K. et al. 1996, *ApJS*, 103, 427
 Griffith, M.R., & Wright, A.E. 1993, *AJ*, 105, 1666
 Klein, U., Mack, K.-H., Gregorini, L. & Vigotti, M., 2003, *A&A*, 406, 579
 Kollgaard, R.I., Palma, C., Laurent-Muehleisen, S.A., Feigelson, E.D., 1996, *ApJ*, 465, 115
 Landt, H., Padovani, P., Perlman, E.S. et al. 2001, *MNRAS*, 323, 757
 Laurent-Muehleisen, S.A., Kollgaard, R.I., Feigelson, E.D. et al. 1999, *ApJ*, 525, 127
 Mantovani, F., Mack, K.-H., Montenegro-Montes, F.M., et al. 2009, *A&A*, 512, 61
 Mantovani, F., Bondi, M. & Mack, K.-H., 2010, *Proceedings of the workshop Fermi meets Jansky – AGN in Radio and Gamma-Rays*, Sovalainen, T., Ros, E., Porcas, R.W., & Zensus, J.A. Editors, June 21–23, 2010, Bonn, Germany, pag. 183
 Marchã, M., 1994, PhD thesis, Univ. Manchester
 Padrielli, L., Aller, M.F., Aller, H.D., et al. 1987, *A&AS*, 67, 63
 Perlman, E.S., Stocke, J.T., Schachter, J.F. et al. 1996, *ApJS*, 104, 251
 Perlman, E.S., Padovani, P., Giommi, P. et al. 1998, *AJ*, 115, 1253
 Stöckel, M., Padovani, P., Urry, C.M. et al. 1991, *ApJ*, 374, 431
 Stocke, J.T., Morris, S.L., Gioia, I.M. et al. 1991, *ApJS*, 76, 813
 White, N.E., & Becker, R.H. 1992, *ApJS*, 79, 331
 White, N.E., Giommi, P., & Angelini, L. 1995
<http://heawww.gsfc.nasa.gov/users.white/wgcat.wgcat.html>
 Wood, K.S., Meekins, J.F., Yentis, D.J. et al. 1984, *ApJS*, 56, 507

Table 1. Flux densities at the available frequencies.

name	RA(J2000)	Dec(J2000)	S _{1.4} mJy	rms mJy	S _{2.64} mJy	rms mJy	S _{4.85} mJy	rms mJy	S _{8.35} mJy	rms mJy	S _{10.45} mJy	rms mJy
J0012.5–1629	00 12 33.83	–16 28 06.8	94.3	2.9	55.1	7.0	49.4	2.5			30.0	6.9
J0015.5+3052	00 15 36.13	+30 52 24.0	234.0	7.0	145.6	3.2	106.7	4.0			51.9	7.9
J0029.0+0509	00 29 03.60	+05 01 34.1	439.8	13.2	362.3	6.2	284.2	10.3			147.9	15.7
J0106.7–1034	01 06 44.09	–10 34 10.0	276.0	9.7	186.4	3.9	150.3	5.6			93.7	10.1
J0110.5–1647	01 10 35.20	–16 48 31.0	105.6	3.7	100.1	3.7	99.1	4.5			95.6	10.8
J0125.0+0146	01 25 05.48	+01 46 26.3	186.6	5.6	152.0	2.8	136.8	5.4			93.1	10.0
J0126.2–0500	01 26 15.36	–05 01 18.5	58.4	2.2	41.1	2.8	32.3	2.3			19.9	5.1
J0204.8+1514	02 04 50.40	+15 14 11.2	4067.7	122.0	2598.1	34.1	2132.2	73.7			1239.9	117.8
J0210.0–1004	02 10 00.14	–10 03 52.8	265.5	8.0	263.8	5.0	200.4	7.6			90.4	11.1
J0227.5–0847	02 27 32.08	–08 48 13.1	65.3	2.0	118.9	2.9	109.5	5.4			66.7	15.4
J0245.2+1047	02 45 15.05	+10 46 53.0	417.4	13.6	289.2	4.4	192.3	6.9			76.0	8.7
J0304.9+0002	03 04 59.23	+00 02 33.4	123.8	4.3	77.6	4.3	53.3	2.6	32.8	5.1	29.0	6.0
J0322.6–1335	03 22 38.45	–13 35 17.8	266.6	8.0			107.3	4.2	87.2	1.8		
J0340.8–1814	03 40 48.05	–18 14 00.0	299.6	10.3	197.6	11.7	135.2	5.9	79.8	2.1		
J0411.0–1637	04 11 00.60	–16 36 07.9	183.5	6.0	152.5	8.7	184.2	6.7	133.8	3.5		
J0414.0–1224	04 14 05.98	–12 24 17.2	93.0	3.3	62.2	6.1	58.7	3.2	47.2	1.9		
J0414.0–1307	04 14 03.14	–13 06 38.9	312.4	9.4	199.9	4.4	136.1	5.0	83.6	1.9		
J0421.5+1433	04 21 33.11	+14 34 03.0	273.2	9.3	163.5	4.4	109.1	4.1	56.5	1.5		
J0427.2–0756	04 27 14.21	–07 56 24.8	74.1	2.6	57.9	2.7	51.1	4.6	45.6	1.3	37.1	7.0
J0434.3–1443	04 34 19.05	–14 42 55.9	205.2	6.2	384.3	5.8	387.9	13.6	297.5	5.2		
J0435.1–0811	04 35 08.38	–08 11 03.2	50.1	1.9	62.7	2.3	91.8	4.5			83.0	9.3
J0447.9–0322	04 47 54.75	–03 22 43.2	86.7	2.6	35.6	3.3	19.6	2.4				
J0502.5+1338	05 02 33.22	+13 38 11.3	544.8	16.3	344.7	5.2	430.0	15.0			327.7	31.6
J0510.0+1800	05 10 02.39	+18 00 41.8	704.3	21.1	533.0	8.1	712.8	24.7	826.8	14.6		
J0513.8+0156	05 13 51.94	+01 56 56.1	348.4	11.7	231.5	5.2						
J0518.2+0624	05 18 15.99	+06 24 22.5	571.0	17.1	375.0	5.7	241.2	8.5	151.6	3.3		
J0535.1–0239	05 35 12.27	–02 39 07.0	46.9	1.9	44.0	15.1	86.4	3.7	72.2	1.7		
J0646.8+6807	06 46 41.50	+68 07 42.9	116.0	4.0	76.9	3.0	72.2	3.1			74.5	8.3
J0651.9+6955	06 51 54.56	+69 55 26.3	275.7	8.3	183.9	3.1	152.1	5.5			109.1	11.1
J0724.3–0715	07 24 17.32	–07 15 19.7	330.4	9.9	255.4	4.3	275.6	9.7	292.4	5.3		
J0744.8+2920	07 44 51.20	+29 20 08.0	337.8	11.8	272.6	4.7	224.9	7.9	168.5	3.2		
J0816.0–0736	08 16 08.48	–07 37 12.3	93.6	2.8	91.7	4.4	41.4	3.1	34.0	6.1		
J0829.5+0858	08 29 30.27	+08 58 21.3	333.9	10.0	234.3	3.6	170.3	6.2	139.7	2.6		
J0847.2+1133	08 47 12.94	+11 33 50.2	32.8	1.1	21.0	2.4	17.6	1.3	17.6	3.6		
J0853.0+2004	08 53 02.75	+20 04 21.5	128.6	3.9	89.4	2.3	67.5	3.1	61.0	2.0		
J0908.2+5031	09 08 16.55	+50 31 05.4	171.6	5.2	102.9	2.7	76.3	3.2			59.7	8.0
J0927.7–0900	09 27 46.93	–09 00 22.2	148.3	4.5	130.8	3.8	91.2	5.2	104.9	2.5		
J0931.9+5533	09 31 58.09	+55 33 13.1	95.7	3.5	101.8	2.8	55.7	3.7			42.7	12.1
J0937.1+5008	09 37 12.32	+50 08 52.2	166.6	5.0	69.1	3.1	110.5	4.3			269.6	26.4
J0940.2+2603	09 40 14.73	+26 03 29.3	462.2	13.9	441.2	6.3	447.6	15.5			378.7	36.4
J1006.1+3236	10 06 07.73	+32 36 27.7	473.8	16.7	282.5	4.9	194.9	7.0			102.4	11.4
J1006.5+0509	10 06 37.64	+05 09 53.5	172.4	5.2	108.2	4.1	126.3	6.6			109.8	12.1
J1010.8–0201	10 10 51.78	–02 00 19.0	532.4	18.4	689.1	9.7	553.0	20.1			499.5	48.1
J1011.5–0423	10 11 30.16	–04 23 29.6	158.4	4.8	151.7	3.9	120.5	5.0			186.9	20.3
J1025.9+1253	10 25 56.34	+12 53 48.8	539.0	16.2	508.6	7.5	654.4	22.7			665.7	63.4
J1026.4+6746	10 26 33.11	+67 46 12.5	234.0	7.9	167.7	3.5	131.6	5.0			92.6	10.5
J1028.5–0236	10 28 34.05	–02 36 59.7	86.6	2.6	98.1	3.2	132.4	5.5			203.0	20.5
J1028.6–0336	10 28 40.37	–03 36 19.4	155.9	4.7	96.7	2.6	60.9	3.5			92.4	14.8
J1032.1–1400	10 32 06.28	–14 00 20.0	195.6	5.9	139.8	4.1	159.3	24.4			134.5	13.9
J1101.8+6241	11 01 53.80	+62 41 56.0	726.5	24.2	462.2	7.1	348.9	12.2			186.5	18.7
J1105.3–1813	11 05 19.19	–18 13 14.0	21.6	0.8	26.5	2.9	34.7	4.3				
J1116.1+0828	11 16 09.96	+08 29 22.1	244.7	7.4	443.7	16.2	397.8	14.8			310.7	30.8
J1120.4+5855	11 20 27.27	+58 56 13.0	90.7	2.7	73.5	2.6	52.4	2.9			36.6	9.5
J1150.4+0156	11 50 24.83	+01 56 19.0	153.2	5.5	120.2	6.7	130.6	7.4			91.7	9.4
J1204.2–0710	12 04 16.70	–07 10 09.6	167.7	6.0	173.5	4.9	150.8	5.6			128.6	14.5
J1206.2+2823	12 06 19.62	+28 22 54.4	37.8	1.2	27.0	2.8	19.7	2.3	18.6	1.2		
J1213.0+3248	12 13 03.81	+32 47 36.8	139.5	4.2	91.7	2.5	66.6	2.7	60.2	1.8		
J1213.2+1443	12 13 15.24	+14 44 02.5	113.5	3.8	77.9	2.6	51.6	2.8	31.5	1.7		
J1217.1+2925	12 17 08.31	+29 25 34.0	66.2	2.0	44.4	3.0	44.4	3.7	41.4	1.4		
J1222.6+2934	12 22 43.14	+29 34 40.4	95.0	2.9	107.0	3.4	110.6	4.3	89.9	3.4		
J1223.9+0650	12 23 54.66	+06 50 02.0	275.7	8.3	266.4	4.4	252.3	8.9			210.1	20.9
J1224.5+2613	12 24 33.39	+26 13 14.3	681.0	21.4	386.9	6.5	238.1	8.4	135.9	2.7		
J1225.5+0715	12 25 31.22	+07 15 52.1	123.9	4.3	75.1	3.8	56.9	2.8			27.7	6.1
J1229.5+2711	12 29 34.26	+27 11 56.8	160.2	4.8	107.8	3.3	123.5	4.8	133.6	2.7		
J1231.7+2848	12 31 43.82	+28 47 50.9	140.5	5.5	147.5	3.4	123.5	5.3	99.2	2.1		
J1311.3–0521	13 11 17.78	–05 21 21.7	69.8	2.5	51.0	6.6	43.3	2.7			37.0	7.8
J1315.1+2841	13 15 13.65	+28 40 52.9	110.3	3.3	118.7	3.5	103.9	4.4	71.1	1.9		
J1320.4+0140	13 20 26.78	+01 40 36.5	670.7	20.1	534.3	7.3	486.0	16.9	491.1	8.8		
J1329.0+5009	13 29 05.87	+50 09 27.0	246.3	7.4	173.8	4.1	178.3	6.4	156.2	3.0		
J1332.7+4722	13 32 45.27	+47 22 22.3	233.2	7.0	222.2	3.7	189.3	6.9	183.9	3.3		
J1337.2–1319	13 37 14.84	–13 19 17.0	113.8	4.1	88.8	2.9	66.6	3.1	60.8	1.5		

name	RA(J2000)	Dec(J2000)	S _{1.4} mJy	rms mJy	S _{2.64} mJy	rms mJy	S _{4.85} mJy	rms mJy	S _{8.35} mJy	rms mJy	S _{10.45} mJy	rms mJy
J1359.6+4010	13 59 38.104	+40 11 37.98	162.8	4.9	199.4	3.1	266.5	9.4	265.3	4.7		
J1400.7+0425	14 00 48.405	+04 25 30.50	322.5	9.7	197.8	3.7	153.9	5.6	150.4	2.8		
J1404.2+3413	14 04 16.732	+34 13 16.10	141.0	4.9	92.3	3.5	55.3	3.1			25.5	3.7
J1406.9+3433	14 06 53.860	+34 33 37.06	169.2	5.1	248.2	3.7	278.1	9.8			189.0	18.8
J1416.4+1242	14 16 28.639	+12 42 13.53	110.2	3.3	95.9	2.6	81.0	3.7	75.7	2.2		
J1417.5+2645	14 17 30.372	+26 44 56.81	75.6	2.3	86.3	2.6	92.4	3.7			82.0	9.2
J1419.1+0603	14 19 09.312	+06 03 30.24	374.6	11.2	283.1	5.8	220.2	7.9	177.7	3.3		
J1420.6+0650	14 20 40.958	+06 51 03.74	533.6	18.2	326.5	4.8	197.9	7.1	129.9	3.0		
J1423.3+4830	14 23 17.955	+48 30 15.47	208.5	6.3			146.8	5.4			103.9	11.1
J1427.9+3247	14 27 58.325	+32 47 40.05	88.0	3.5	98.2	2.8	60.5	3.0			31.1	6.0
J1442.3+5236	14 42 19.598	+52 36 21.09	187.2	5.6	132.2	3.0	95.0	3.6			51.3	6.3
J1507.9+6214	15 07 57.346	+62 13 34.64	549.7	16.5	327.9	5.0	213.9	7.6			103.4	11.3
J1539.1-0658	15 39 09.627	-06 58 43.58	46.8	1.5	71.1	3.3	83.5	4.6	77.0	2.1		
J1543.6+1847	15 43 43.810	+18 47 20.31	356.2	10.7	206.8	3.9	166.4	5.9			127.3	12.9
J1606.0+2031	16 06 05.922	+20 32 09.27	180.8	5.4	105.2	3.3	81.6	3.3	66.8	1.6		
J1626.6+5809	16 26 37.429	+58 09 11.48	532.9	18.3	400.6	5.8	359.7	12.5	298.9	5.5		
J1629.7+2117	16 29 47.534	+21 17 17.51	264.4	7.9	151.9	3.4	97.6	3.9	55.6	1.4		
J1648.4+4104	16 48 29.314	+41 04 05.84	243.0	7.3	373.8	5.6	499.9	17.4	534.5	9.4		
J1656.6+5321	16 56 39.687	+53 21 48.51	94.4	2.9	135.9	2.8	134.3	5.3	112.6	3.2		
J1656.8+6012	16 56 48.308	+60 12 16.09	292.2	8.8	475.5	7.1	484.7	16.8	435.0	7.8		
J1722.3+3103	17 22 18.547	+31 03 26.23	129.4	4.2	82.5	2.9	51.7	2.3	29.4	1.3		
J1804.7+1755	18 04 42.496	+17 55 58.76	218.0	7.2	152.5	3.2	104.1	4.0	59.8	1.4		
J1840.9+5452	18 40 57.444	+54 52 14.12	207.3	7.3	188.4	4.2	195.1	7.1	191.6	3.4	180.0	17.6
J2109.7-1332	21 09 49.865	-13 32 46.21	61.9	1.9	46.4	3.2	36.7	2.2			26.3	6.2
J2154.1-1501	21 54 07.563	-15 01 23.14	311.5	9.9	235.0	5.9	241.2	8.8			149.7	5.1
J2159.3-1500	21 59 20.202	-15 00 35.52	82.5	2.5	90.1	3.2	68.2	3.1			25.9	14.9
J2239.7-0631	22 39 46.534	-06 31 57.37	117.2	4.2	84.4	3.6	89.9	4.0			54.9	6.9
J2320.6+0032	23 20 37.954	+00 31 40.10	82.0	2.5	77.9	3.3	96.1	3.8	85.1	1.9		
J2322.0+2114	23 22 01.946	+21 13 50.17	151.6	4.9	92.5	2.5	76.6	4.5	38.1	1.4		
J2329.0+0834	23 29 05.799	+08 34 15.22	172.9	5.2	222.5	4.2	293.6	10.3	313.8	7.3		
J2333.2-0131	23 33 16.675	-01 31 07.61	258.3	7.8	145.4	3.9	143.5	5.4	146.4	2.7		
J2347.6+0852	23 47 37.444	+08 52 56.58	147.7	5.4	93.4	3.1	72.1	3.1			39.8	5.5

The table is organised as follows: col. 1: source name; cols. 2 and 3: right ascension and declination in J2000 coordinates, taken from FIRST or NVSS images; cols. 4–13: flux density measurements and associated errors at the NVSS and Effelsberg 100-m telescope observing frequencies.

Table 2. Spectral index classification.

Sp.In. type	No.	%	notes
Steep $\alpha \leq -0.5$	27	26.2	16 with $\alpha < -0.7$
Steep-flat	18	17.5	
Flat-steep	4	3.9	
Flat	37	35.9	
GPS	9	8.7	
Inverted	7	6.8	
Undefined	1	1	

Table 3. Variability and spectral class.

name	z	O.I.	S_{G-P} mJy	rms mJy	S_{EF}/S_{G-P}	$R_{87/90-09}$	R_{86-87}	S.I.	comments
J0012.5-1629	0.151	FSRQ	50	14	0.99	0.04		steep	SSRQ
J0015.5+3052	1.619	FSRQ	89	12	1.20	2.60		steep +	SSRQ
J0029.0+0509	1.633	FSRQ	377	49	0.75	2.10		flat-steep	break at ~5 GHz
J0106.7-1034	0.469	FSRQ	188	16	0.80	2.22		steep	SSRQ
J0110.5-1647	0.780	FSRQ	72	14	1.37	1.84		flat	
J0125.0+0146	1.559	FSRQ	95	13	1.45	4.63		flat	
J0126.2-0500	0.411	FSRQ	54	13	0.60	1.64		steep	SSRQ
J0204.8+1514	0.405	FSRQ	3073	273	0.69	2.57		steep	SSRQ
J0210.0-1004	1.976	FSRQ	244	18	0.82	2.23		flat-steep	break at ~2.7 GHz
J0227.5-0847	2.228	FSRQ	115	14	0.95	0.36		GPS	peak at ~3.2 GHz
J0245.2+1047	0.070	BLLac	217	19	0.89	0.55		steep	SS-BLLac
J0304.9+0002	0.563	FSRQ	75	?	0.71	1.52		steep	SSRQ
J0322.6-1335	1.468	FSRQ	164	16	0.65	3.42		steep	SSRQ
J0340.8-1814	0.195	RG ?	148	16	0.91	0.75		steep	SS-RG
J0411.0-1637	0.622	FSRQ	124	15	1.48	3.66		flat	
J0414.0-1224	0.463	FSRQ	152	16	0.39	5.71		steep +	SSRQ
J0414.0-1307	0.569	FSRQ	42	14	3.24	6.32		steep-flat	break at ~2.7 GHz
J0421.5+1433	?	BLLac	114	11	0.96	0.50		steep +	SS-BLLac
J0427.2-0756	1.375	FSRQ	56	13	0.91	0.35		flat	
J0434.3-1443	1.899	FSRQ	281	20	1.38	4.41		GPS	break at ~3.2 GHz
J0435.1-0811	0.791	FSRQ	73	13	1.26	1.36		GPS	possibly inverted
J0447.9-0322	0.774	FSRQ	56	13	0.35	2.75		steep +	SSRQ
J0502.5+1338	?	BLLac	459	41	0.94	1.69	2.12	steep-flat	break at ~2.7 GHz
J0510.0+1800	0.416	FSRQ	796	71	0.90	0.89		flat	
J0513.8+0156	0.084	BLLac	131	13				-	
J0518.2+0624	0.891	FSRQ	230	21	1.05	0.10		steep +	SSRQ
J0535.1-0239	1.033	FSRQ	42	13	2.06	3.28		inverted	
J0646.8+6807	0.927	FSRQ	72	7	1.00	0.36		steep-flat	
J0651.9+6955	1.367	FSRQ	132	12	1.15	2.58		flat	
J0724.3-0715	0.270	FSRQ	482	28	0.57	6.96		flat	
J0744.8+2920	1.168	FSRQ	179	16	1.26	3.74		flat	
J0816.0-0736	0.040	BLLac	61	13	0.68	1.46		flat-steep	break at ~2.7 GHz
J0829.5+0858	0.866	FSRQ	180	16	0.95	0.15		flat	
J0847.2+1133	0.119	BLLac	32	5	0.55	1.74		steep-flat	break at ~2.7 GHz
J0853.0+2004	1.930	SSRQ	60	6	1.13	0.05		steep-flat	break at ~3.0 GHz
J0908.2+5031	0.917	SSRQ	86	8	0.89	1.00		steep-flat	break at ~3.0 GHz
J0927.7-0900	0.254	FSRQ	181	16	0.50	5.33		flat	
J0931.9+5533	0.266	SSRQ	53	6	1.05	0.97		GPS	peak at ~2.7 GHz
J0937.1+5008	0.275	FSRQ	315	28	0.35	11.2		inverted ?	peculiar spectral index
J0940.2+2603	0.498	FSRQ	292	26	1.53	4.60		flat	
J1006.1+3236	1.020	SSRQ	231	21	0.84	2.77		steep +	
J1006.5+0509	1.216	FSRQ	179	16	0.71	3.10		steep-flat	break at ~2.7 GHz
J1010.8-0201	0.896	FSRQ	826	45	0.67	5.53		flat	
J1011.5-0423	1.588	FSRQ	189	16	0.64	4.08		flat	
J1025.9+1253	0.663	FSRQ	631	56	1.04	0.14		flat	
J1026.4+6746	1.181	FSRQ	129	12	1.02	0.15		flat	
J1028.5-0236	0.476	FSRQ	94	13	1.41	2.72		inverted	
J1028.6-0336	1.781	SSRQ	61	13	1.00	0.001		steep-flat	possibly inverted at higher frequencies
J1032.1-1400	1.039	FSRQ	223	18	0.71	2.10		flat	
J1101.8+6241	0.663	FSRQ	693	61	0.50	9.41		steep	SSRQ
J1105.3-1813	0.578	FSRQ	59	14	0.59	1.65		inverted	
J1116.1+0828	0.486	FSRQ	282	25	1.41	3.42		GPS	peak at ~2.7 GHz
J1120.4+5855	0.158	NLRG	46	5	1.14	0.05		flat	
J1150.4+0156	1.502	FSRQ	95	10	1.38	2.80		flat	
J1204.2-0710	0.185	BLLac	128	15	1.18	1.42		flat	
J1206.2+2823	0.708	FSRQ	21	4	0.94	1.12		steep-flat	break at ~5.0 GHz
J1213.0+3248	2.502	FSRQ	61	6	1.09	0.54		steep-flat	break at ~5.0 GHz
J1213.2+1443	0.718	SSRQ	61	7	0.85	1.42		steep +	
J1217.1+2925	0.974	FSRQ	49	6	0.91	0.55		steep-flat	break at ~2.7 GHz
J1222.6+2934	0.401	SSRQ	60	6	1.84	5.79		flat	
J1223.9+0650	1.189	FSRQ	251	23	1.01	1.25		flat	
J1224.5+2613	0.687	FSRQ	272	24	0.88	0.29		steep +	SSRQ
J1225.5+0715	1.120	SSRQ	75	9	0.76	0.09		steep +	
J1229.5+2711	0.490	NLRG	165	15	0.75	1.97	2.79	steep-flat	break at ~2.7 GHz; possibly inverted
J1231.7+2848	?	BLLac	114	11	1.08	1.19		flat	
J1311.3-0521	0.160	BLLac	46	13	0.94	0.20		flat	
J1315.1+2841	1.576	FSRQ	95	9	1.09	1.88		flat-steep	possibly GPS, break at ~5.0 GHz
J1320.4+0140	1.235	BLLac	541	48	0.90	1.07		flat	
J1329.0+5009	2.650	SSRQ	133	12	1.34	3.31		steep-flat	break at ~2.7 GHz
J1332.7+4722	0.668	SSRQ	333	29	0.57	4.72	3.50	flat	
J1337.2-1319	3.475	FSRQ	71	14	0.94	0.30		flat	

name	z	O.I.	S_{G-P} mJy	rms mJy	S_{EF}/S_{G-P}	$R_{87/90-09}$	R_{86-87}	S.I.	comments
J1359.6+4010	0.407	FSRQ	281	25	0.95	0.96			inverted
J1400.7+0425	2.550	FSRQ	267	24	0.58	4.52			steep-flat break at ~ 2.7 GHz
J1404.2+3413	0.937	SSRQ	62	6	0.89	1.36			steep +
J1406.9+3433	2.556	FSRQ	204	18	1.36	3.96			GPS peak at ~ 5.0 GHz
J1416.4+1242	0.335	FSRQ	98	10	0.83	2.32			flat
J1417.5+2645	1.455	FSRQ	77	8	1.20	1.89			flat
J1419.1+0603	2.389	FSRQ	240	22	0.92	3.94	2.85		flat
J1420.6+0650	0.236	FSRQ	241	9	0.82	1.34			steep + SSRQ
J1423.3+4830	0.569	SSRQ	100	9	1.47	4.36			flat
J1427.9+3247	0.568	SSRQ	65	7	0.93	1.69			GPS peak at ~ 2.7 GHz
J1442.3+5236	1.800	FSRQ	111	10	0.86	1.54			steep SSRQ
J1507.9+6214	1.478	SSRQ	213	19	1.00	0.07			steep +
J1539.1-0658	?	BLLac	76	13	1.10	0.54			GPS peak at ~ 5.0 GHz
J1543.6+1847	1.396	FSRQ	300	27	0.55	5.77			steep-flat break at ~ 2.7 GHz
J1606.0+2031	0.383	FSRQ	196	18	0.42	6.70			steep-flat break at ~ 2.7 GHz
J1626.6+5809	0.748	SSRQ	315	28	1.14	1.58			flat
J1629.7+2117	0.833	FSRQ	105	10	0.93	0.78			steep + SSRQ
J1648.4+4104	0.851	SSRQ	197	18	2.54	14.4			inverted
J1656.6+5321	1.555	FSRQ	145	13	0.93	2.92	4.62		flat possibly GPS
J1656.8+6012	0.623	FSRQ	184	16	2.63	17.4	5.16		flat possibly GPS
J1722.3+3103	0.305	SSRQ	53	6	0.98	0.63			steep +
J1804.7+1755	0.435	FSRQ	92	9	1.13	1.30			steep + SSRQ
J1840.9+5452	0.646	BLLac	252	22	0.77	3.54			flat
J2109.7-1332	1.226	FSRQ	51	14	0.72	1.00			flat
J2154.1-1501	1.208	FSRQ	219	18	1.10	1.10			flat possibly flat-steep
J2159.3-1500	2.270	FSRQ	86	14	0.79	1.24			GPS peak at ~ 2.7 GHz
J2239.7-0631	0.264	SSRQ	64	13	1.40	1.90			flat-steep break at ~ 3.5 GHz
J2320.6+0032	1.894	FSRQ	87	10	1.10	0.88			flat
J2322.0+2114	0.707	FSRQ	100	9	0.77	1.67			steep + SSRQ
J2329.0+0834	0.948	FSRQ	273	24	1.08	0.45	4.13		inverted
J2333.2-0131	1.062	FSRQ	314	21	0.46	7.86			steep-flat break at ~ 2.7 GHz
J2347.6+0852	0.292	FSRQ	154	7	0.47	2.00			steep SSRQ

The table is organised as follows: col. 1: source name; cols. 2 and 3: redshift and spectral class respectively, taken from Perlman et al. (1998) and Landt et al. (2001); col. 4: GB6 flux density at 4.85 GHz for sources with $0^\circ < \text{Dec.} < 75^\circ$ and PMN flux density at 4.85 GHz for sources with $-20^\circ < \text{Dec.} < 0^\circ$ taken from Perlman et al. (1998) and Landt et al. (2001); col. 5: rms error; col. 6: Effelsberg to GB6 or PMN flux density ratio; col. 7: R parameter for the long-term variability; col. 8: R parameter for the short-term variability; col. 9: spectral index type; col. 10: new spectral index classification and comments.

name	$m_{1.4}$ %	Δm %	$\chi_{1.4}$ °	$\Delta\chi$ °	$m_{2.64}$ %	Δm %	$\chi_{2.64}$ °	$\Delta\chi$ °	$m_{4.85}$ %	Δm %	$\chi_{4.85}$ °	$\Delta\chi$ °	$m_{8.35}$ %	Δm %	$\chi_{8.35}$ °	$\Delta\chi$ °	$m_{10.45}$ %	Δm %	$\chi_{10.45}$ °	$\Delta\chi$ °	RM rad m ⁻²	
J1359.6+4010	< 0.8				< 3				< 2				< 1									
J1400.7+0425	1.3	0.2	-9.8	2.1	4.1	0.9	118.7	8.0	4.9	1.1	-22.7	8.0	3.2	0.5	-16.5	6.8						-60.5
J1404.2+3413	5.8	0.6	72.6	1.1	< 3				< 2								< 1					
J1406.9+3433	1.3	0.3	85.2	3.8	< 3				1.7	0.5	-69.3	11.7					< 1					
J1416.4+1242	4.0	0.5	-5.8	2.0	< 3				< 2				< 1									
J1417.5+2645	1.9	0.6	-5.2	5.7	< 3				< 2								< 1					
J1419.1+0603	0.4	0.1	-49.1	5.5	< 3				4.1	1.0	-27.4	8.7	2.9	0.5	-12.9	7.9						-84.3
J1420.6+0650	5.4	0.4	-25.4	0.5	6.2	0.6	150.3	4.0	7.2	1.1	-27.1	5.6	4.5	0.7	-23.3	6.1						-0.5 ?
J1423.3+4830	1.2	0.2	-3.2	3.1	< 2				< 2								< 1					
J1427.9+3247	< 1.8				< 3				< 2								< 1					
J1442.3+5236	4.9	0.4	-89.8	0.9	3.8	1.3	208.1	13.1	< 2								< 1					
J1507.9+6214	0.9	0.1	65.6	1.7	2.0	0.6	187.2	10.8	< 2								< 1					
J1539.1-0658	< 3.0				< 3				< 2				< 1									
J1543.6+1847	3.5	0.2	-59.1	0.7	6.3	0.9	96.3	5.3	6.2	1.1	81.7	6.1					< 1					-13.6
J1606.0+2031	5.4	0.4	44.9	0.9	5.4	1.8	170.1	13.0	7.2	1.8	-27.8	9.5	5.1	1.4	-26.3	10.7						29.0
J1626.6+5809	0.5	0.1	-85.9	3.0	2.1	0.4	203.9	8.0	2.1	0.5	32.3	8.7	1.4	0.3	34.9	7.7						-50.2
J1629.7+2117	< 0.5			3.8	1.1	97.4	11.1	< 2					< 1									
J1648.4+4104	2.2	0.2	69.9	1.6	< 3				1.7	0.4	18.2	9.0	3.4	0.2	-2.2	2.0						170.0
J1656.6+5321	1.8	0.5	-42.2	4.4	< 3				< 2				4.0	0.8	107.0	8.3						
J1656.8+6012	0.7	0.2	-25.2	3.9	3.9	0.3	147.0	3.5	4.9	0.3	133.6	2.5	3.1	0.2	129.8	2.3						10.9
J1722.3+3103	< 2.5				< 3				< 2				< 1									
J1804.7+1755	3.8	0.5	54.2	1.5	< 3				6.7	1.3	-51.8	7.8	< 1									
J1840.9+5452	3.1	0.3	84.6	1.3	5.1	1.5	261.5	11.0	< 2								< 1					
J2109.7-1332	< 2.2				< 3				< 2				< 1									
J2154.1-1500	2.3	0.4	-54.5	2.0	4.6	1.2	92.7	10.3	3.1	0.6	-91.7	8.7					< 1					15.4
J2159.3-1501	< 1.6				< 3				< 2													
J2239.7-0631	< 0.4				< 3				< 2													
J2320.6+0032	2.9	0.7	2.8	3.8	< 3				< 2													
J2322.0+2114	< 7.1				< 3				< 2				< 1									
J2329.0+0834	1.9	0.3	-8.1	2.6	< 3				< 2				< 1									
J2333.2-0131	1.7	0.2	64.2	2.1	< 3				< 2				4.6	0.7	91.7	5.2						
J2347.6+0852	7.0	0.9	8.4	1.2	< 3				< 2				2.8	0.6	-26.1	9.2						

The table is organised as follows: col. 1: source name; cols. 2 and 3: percentage of polarised flux density and associated error, cols. 4 and 5: EVPA χ and associated error at 1.4 GHz extracted from Condon et al. (1998); cols. 6–9: percentage of polarised flux density and associated error, χ and associated error at 2.64 GHz; cols. 10–13: percentage of polarised flux density and associated error, χ and associated error at 4.85 GHz; cols. 14–17: percentage of polarised flux density and associated error, χ and associated error at 8.35 GHz; 10.45 GHz respectively; cols. 18–21: percentage of polarised flux density and associated error, χ and associated error at 10.45 GHz; col. 22: rotation measure (observer's frame)

Table 5. Comparison between percentage of polarised emission for different samples of objects.

Freq.(GHz)	m blazars	m B3-VLA	m CSS
1.4	3.0 ^{+0.4} _{-0.8}	2.2	1.6 ^{+2.2} _{-1.0}
2.64	4.9 ^{+1.1} _{-0.4}	3.7	4.2 ^{+6.1} _{-0.6}
4.85	5.8 ± 0.9	5.2	3.7 ^{+5.7} _{-1.0}

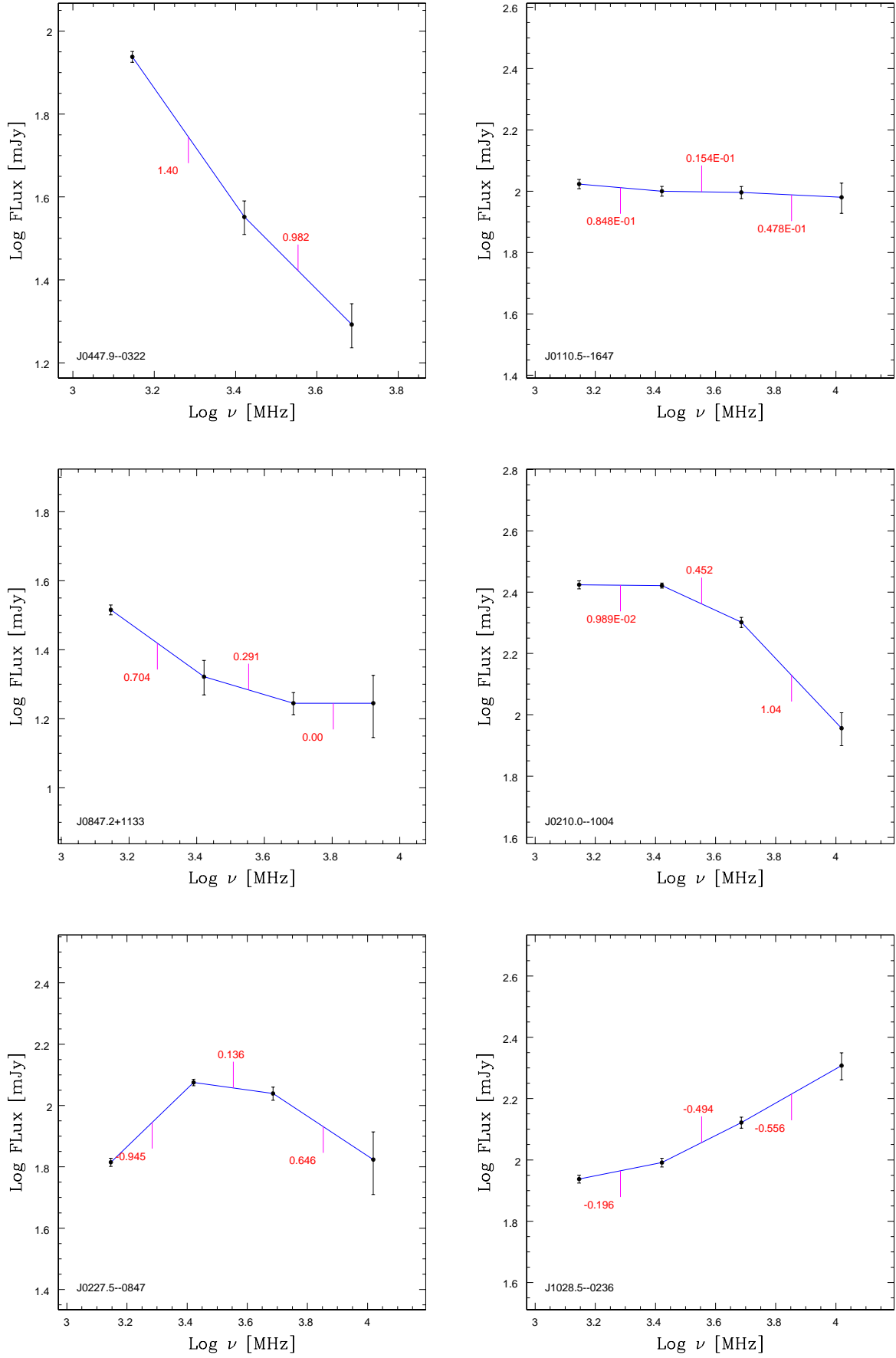


Fig. 1. Examples of spectral index behaviour, namely: “steep” (J0447.9–0322), “flat” (J0110.5–1647), “steep–flat” (J0847.2+1133), “flat–steep” (J0210.0–1004), “GPS” (J0227.5–0847), “inverted” (J1028.5–0236).

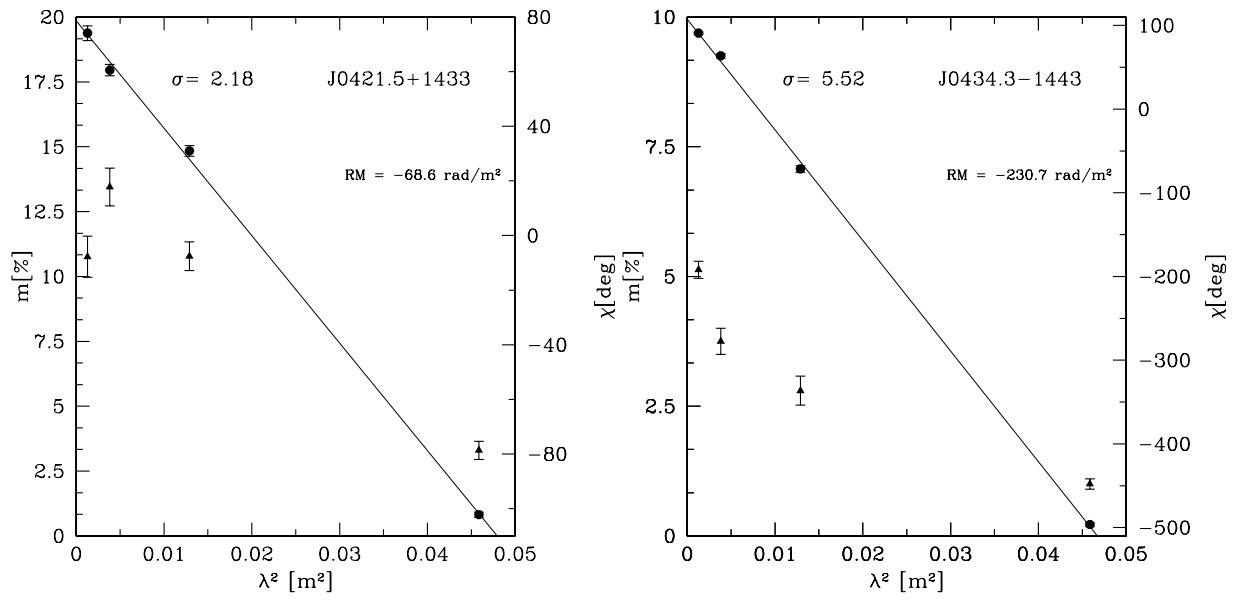


Fig. 2. Examples of position angles of the electric vector χ (dots) and fractional polarisation m (triangles) versus λ^2 plot. σ values assess the quality of the best fit.

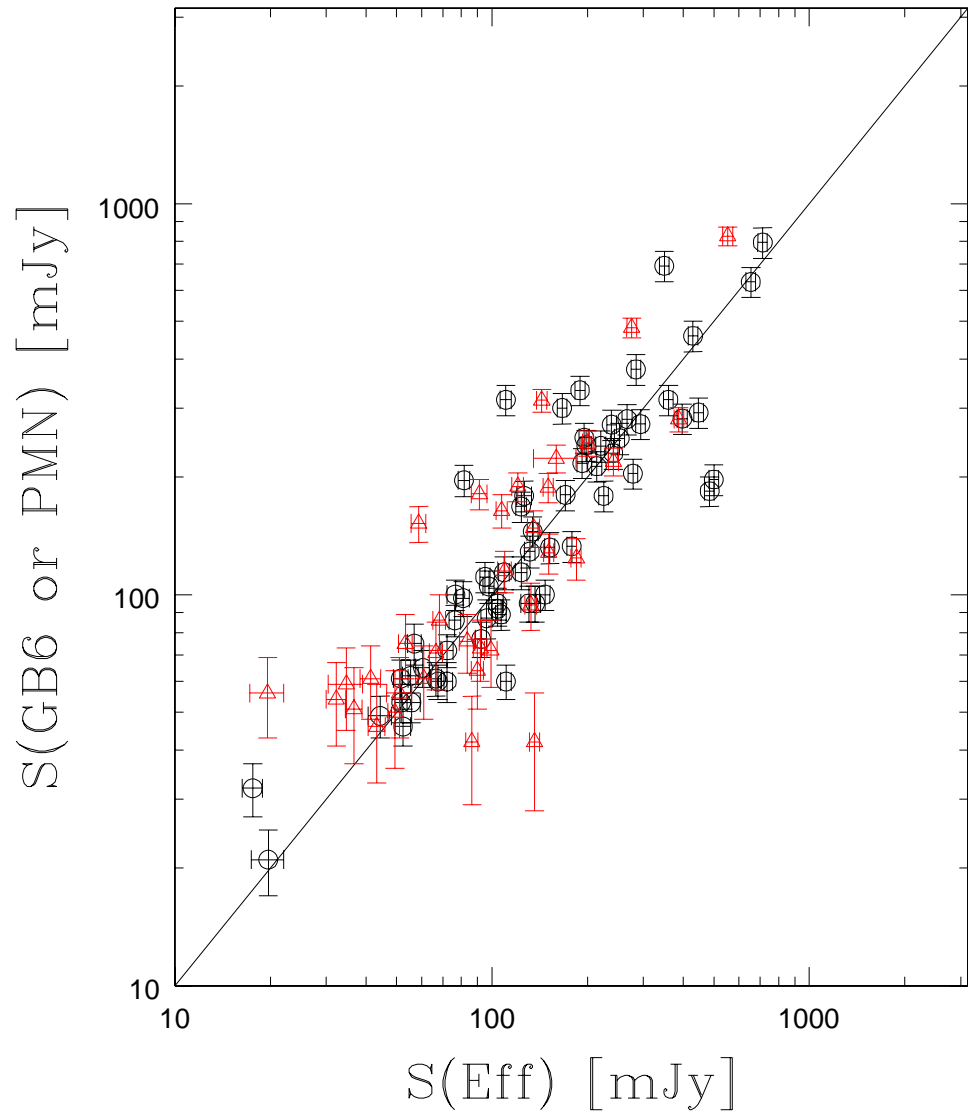


Fig. 3. Effelsberg flux densities versus GB6 (points) or PMN (triangles) flux densities at 5 GHz. The straight line means a ratio of 1.

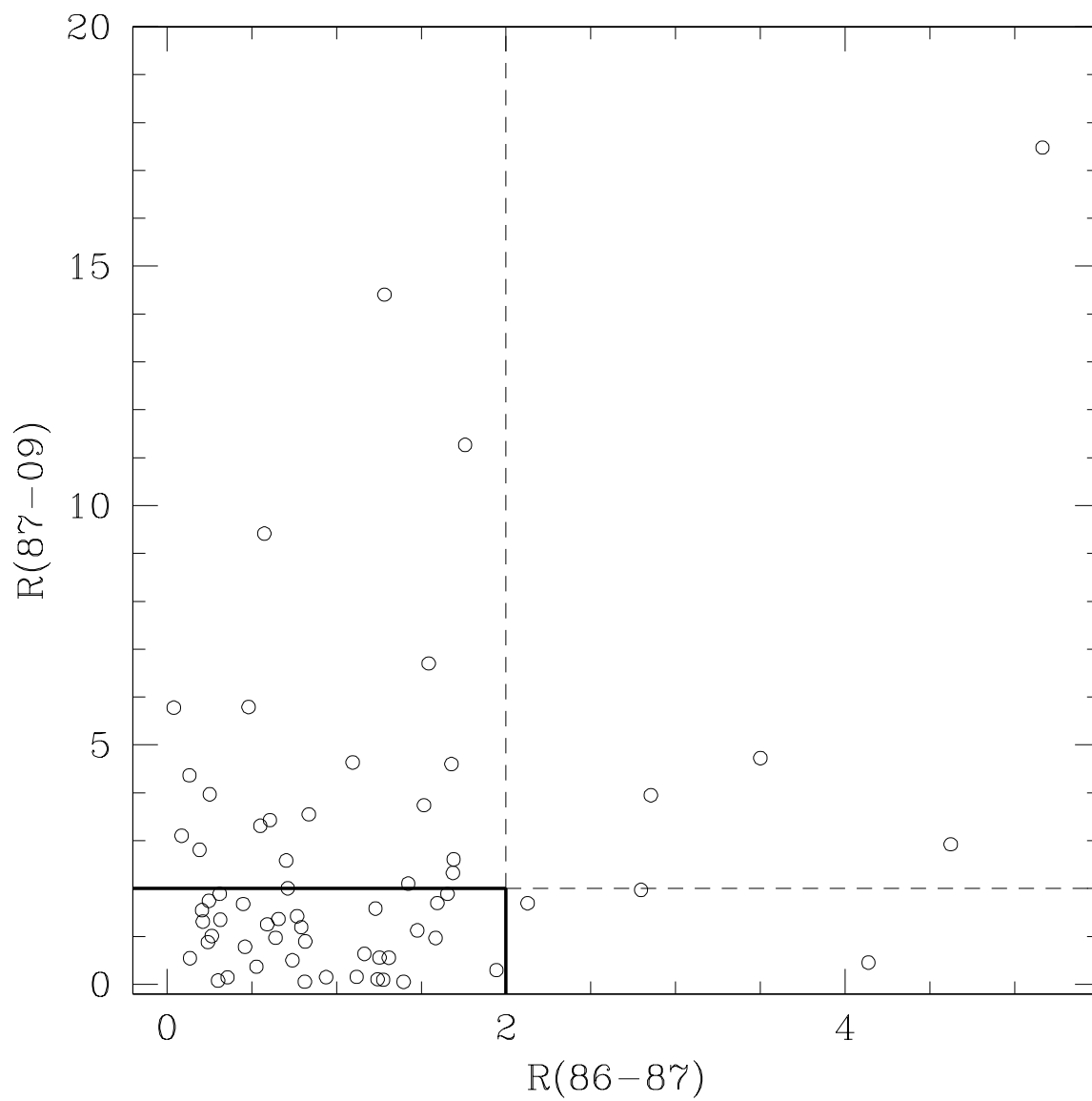


Fig. 4. The R values for both short and long-term variability.

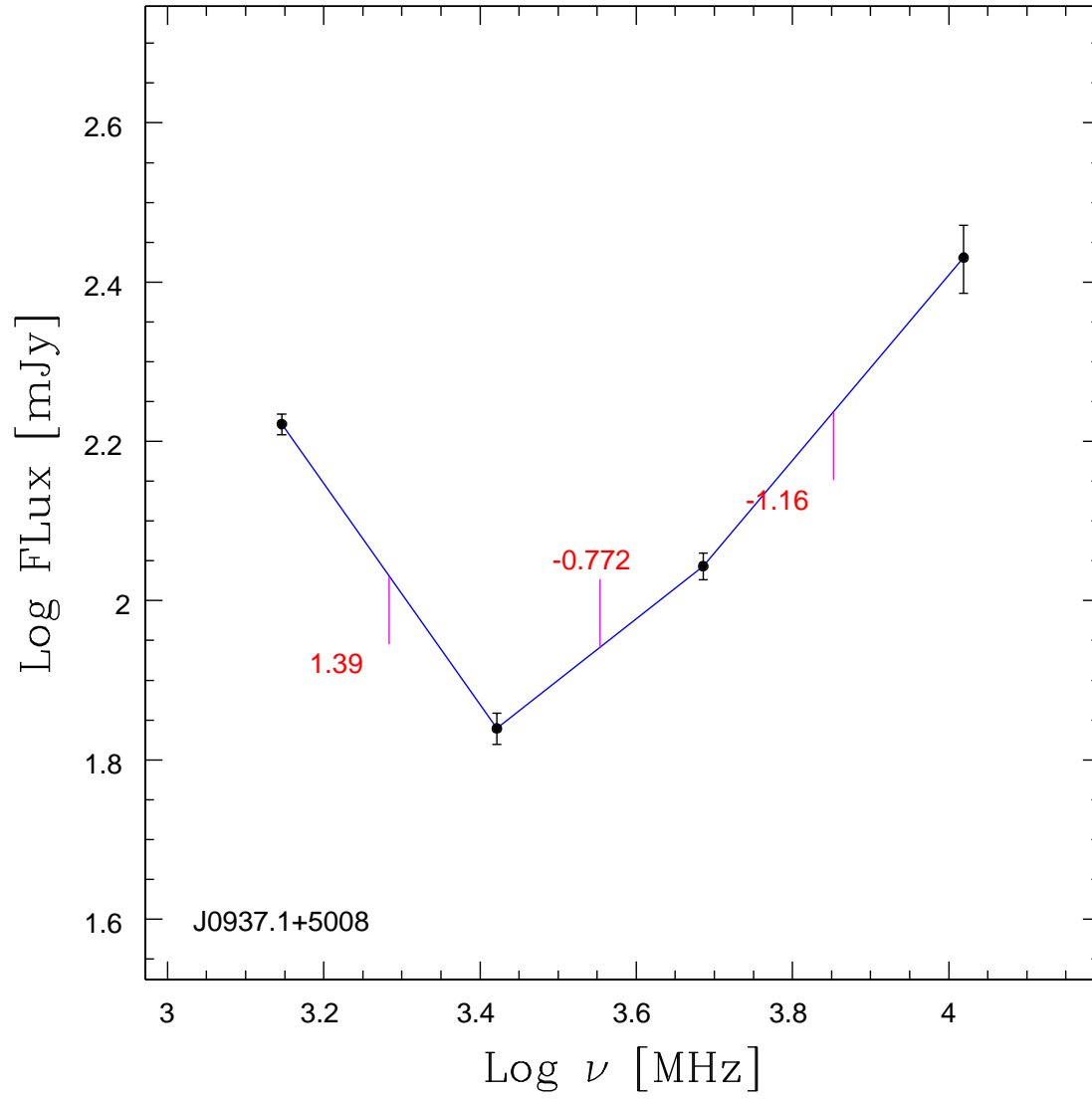


Fig. 5. The “concave” spectral index of the source J0937.1+5008.

Appendix A: Spectral index plots

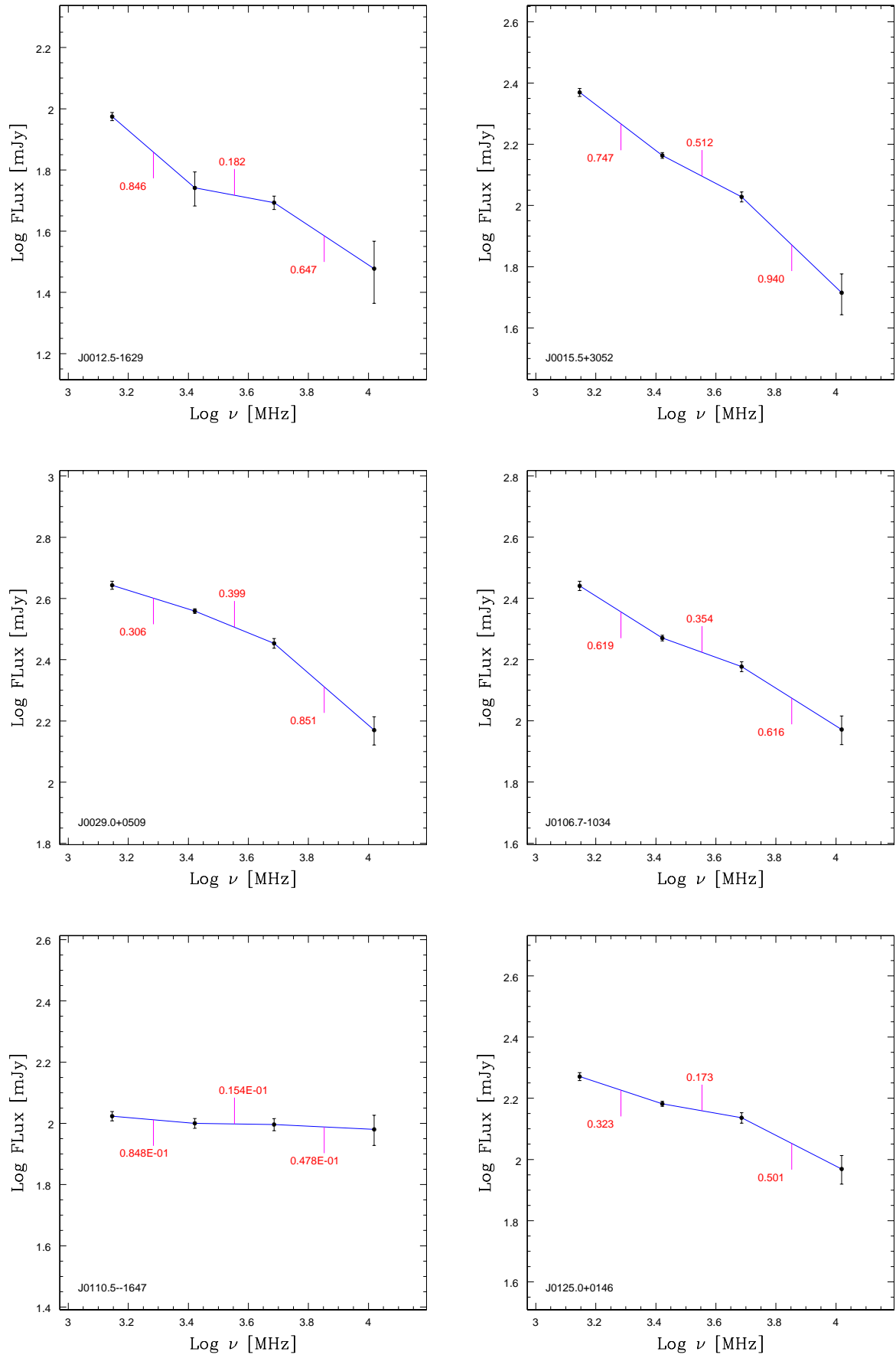


Fig. A.1. Spectral index plots of sources in Table 3.

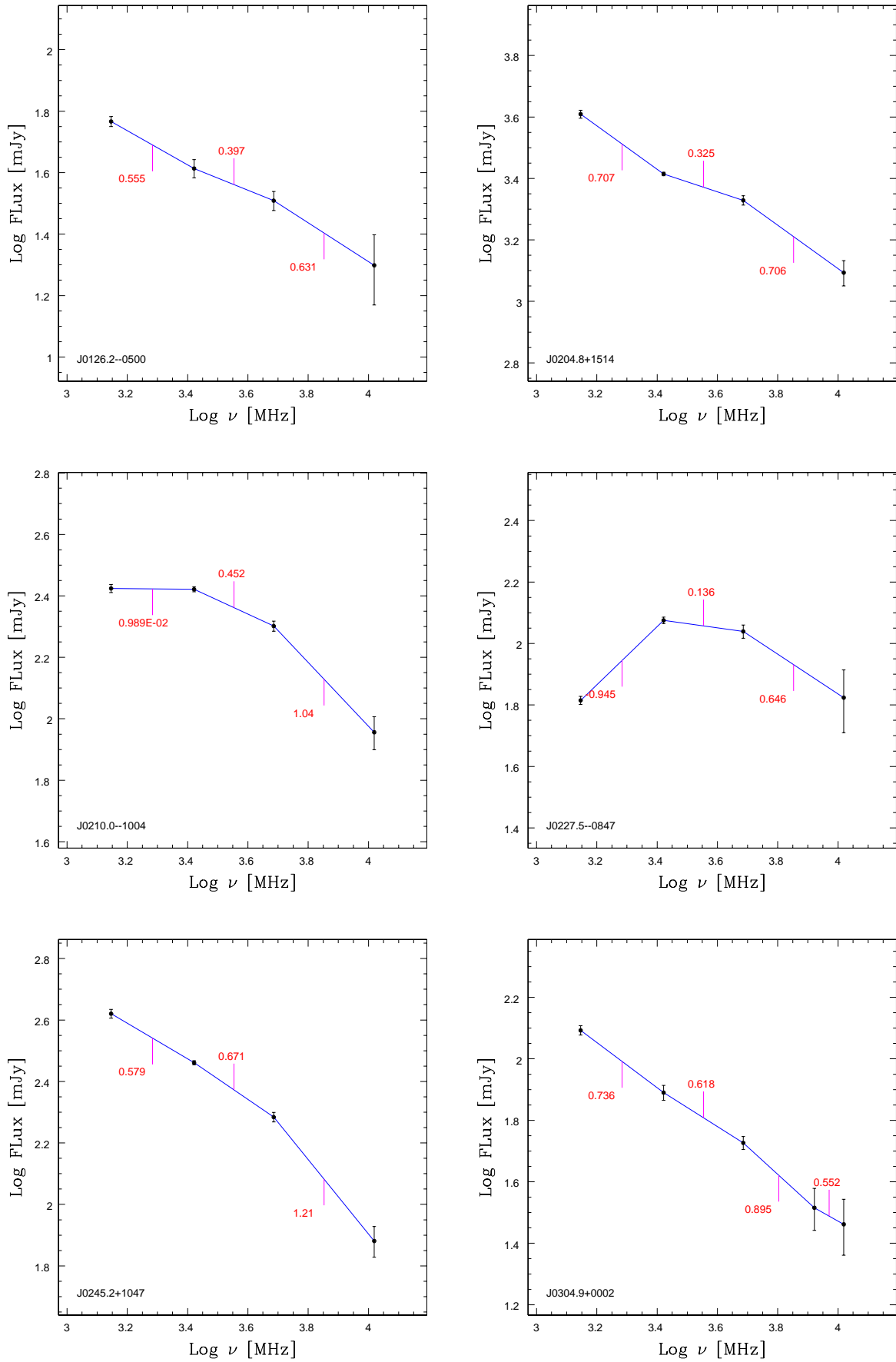


Fig. A.2. Spectral index plots of sources in Table 3.

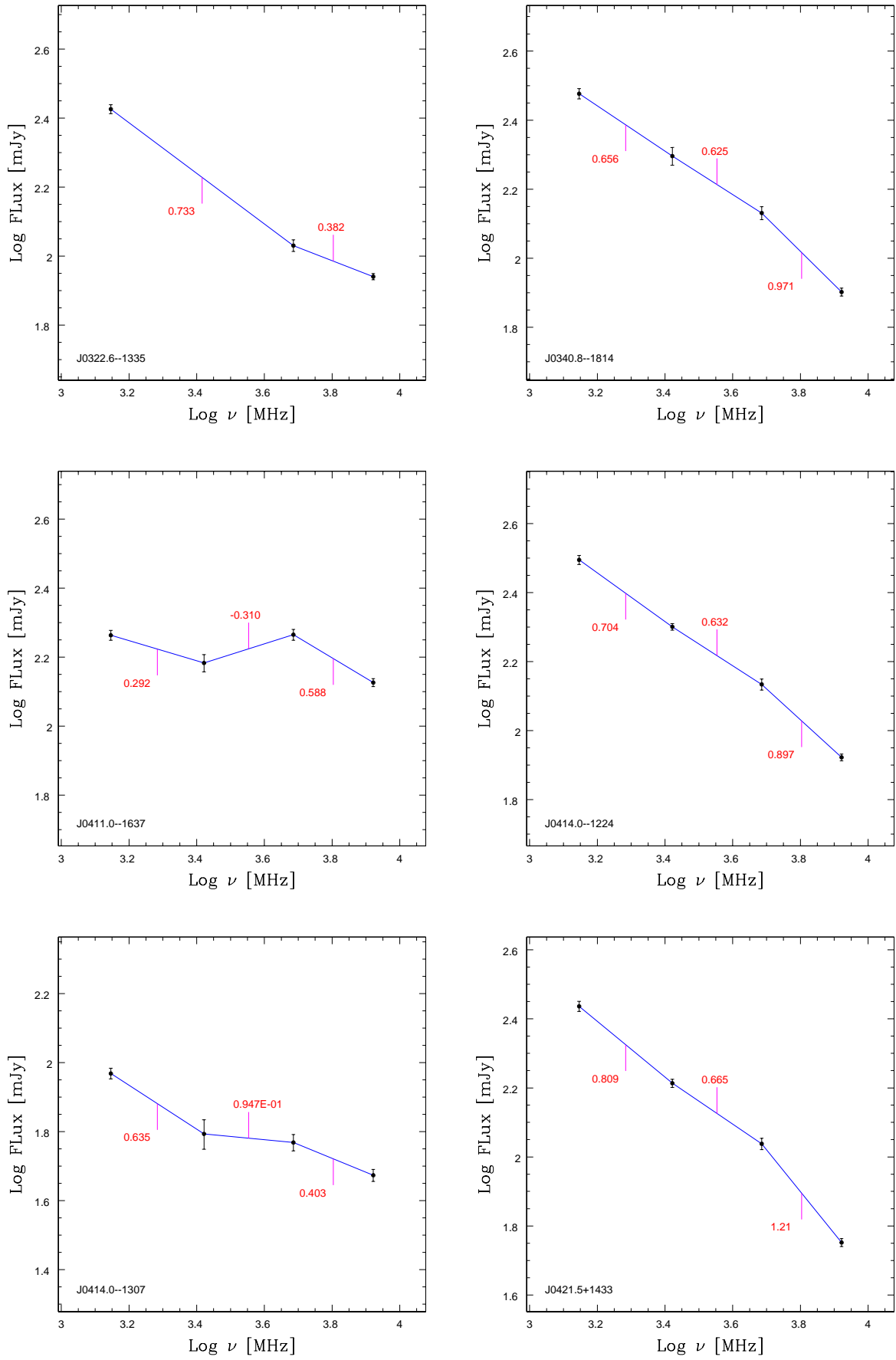


Fig. A.3. Spectral index plots of sources in Table 3.

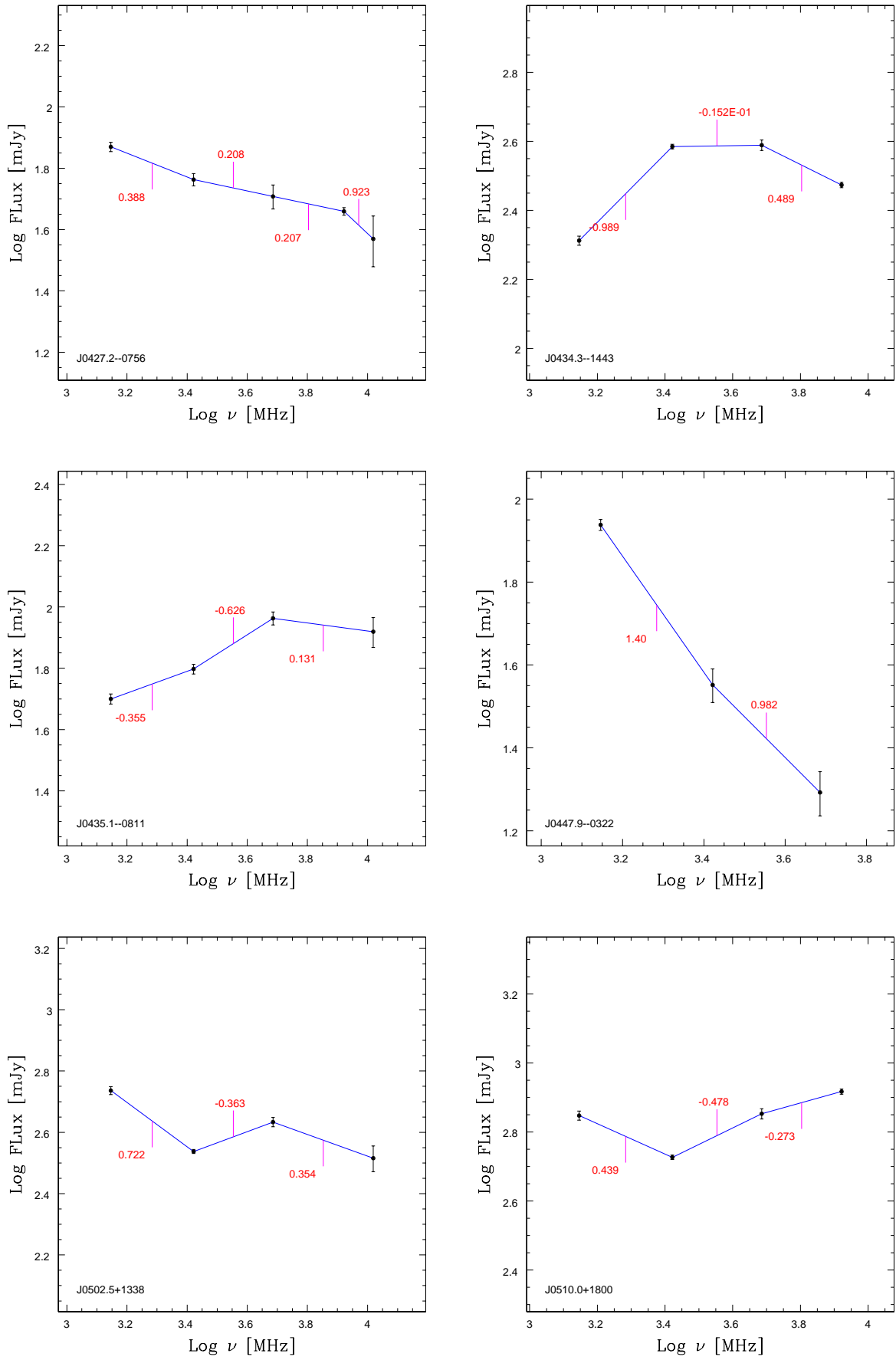


Fig. A.4. Spectral index plots of sources in Table 3.

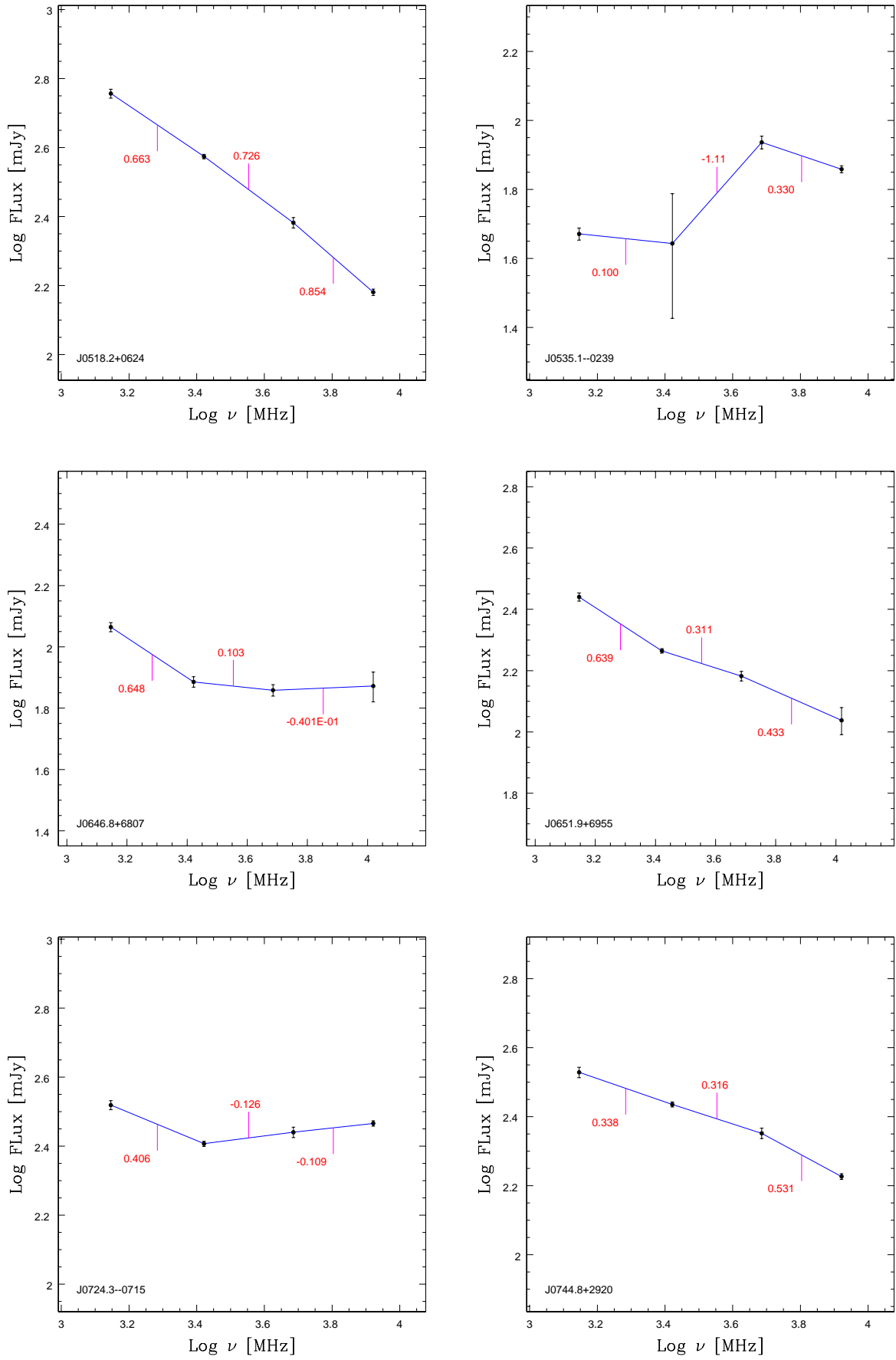


Fig. A.5. Spectral index plots of sources in Table 3.

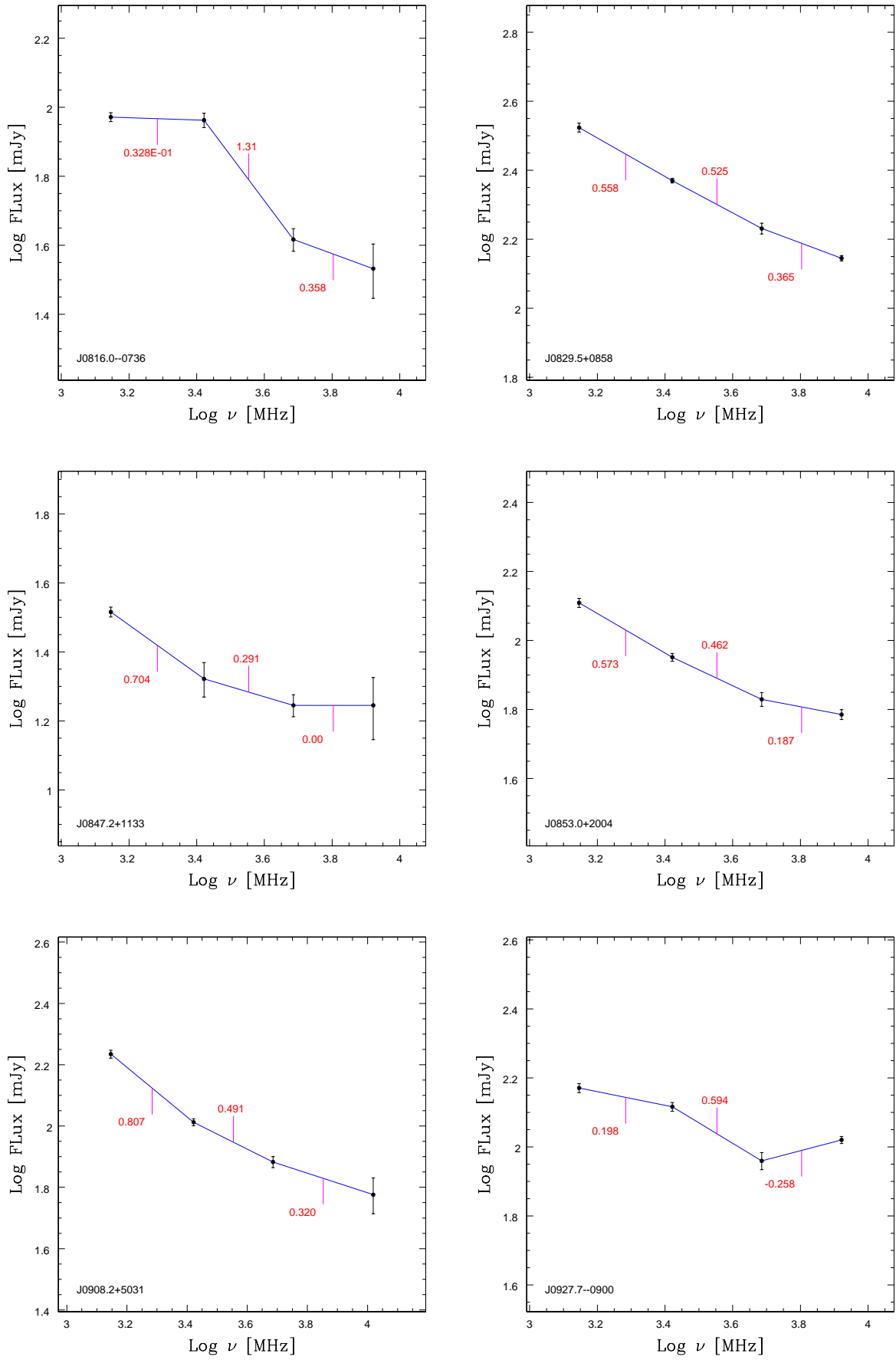


Fig. A.6. Spectral index plots of sources in Table 3.

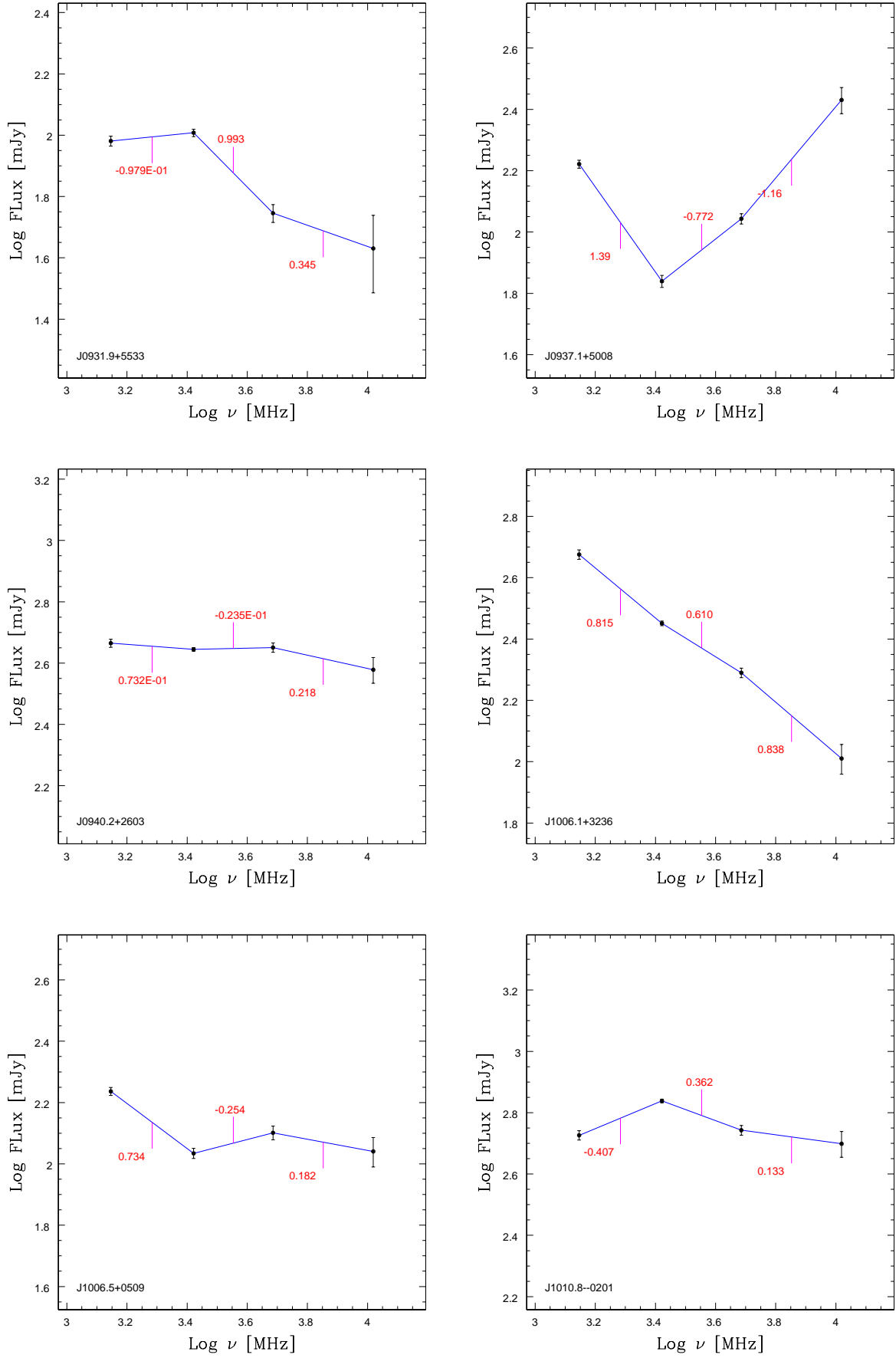


Fig. A.7. Spectral index plots of sources in Table 3.

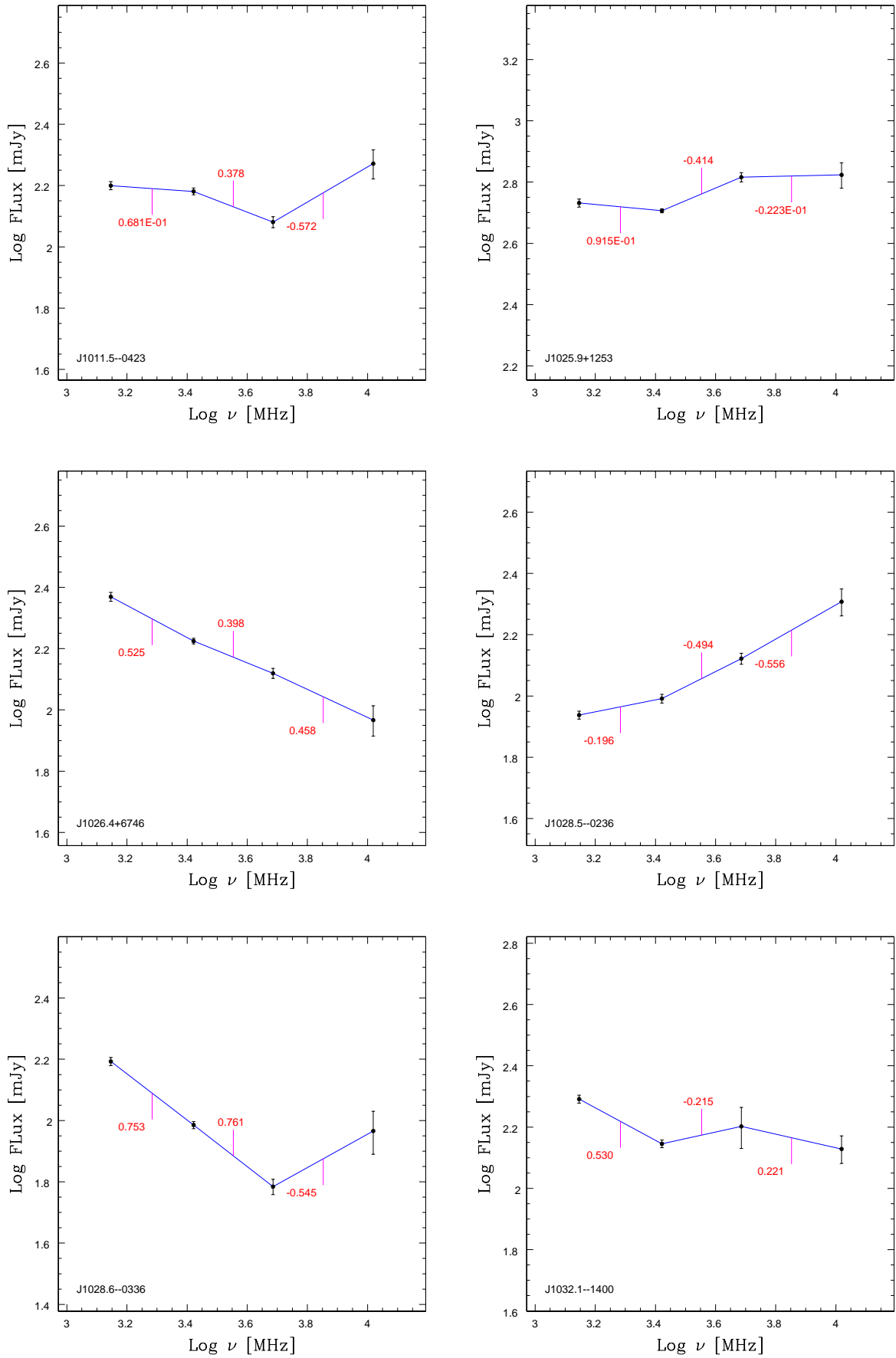


Fig. A.8. Spectral index plots of sources in Table 3.

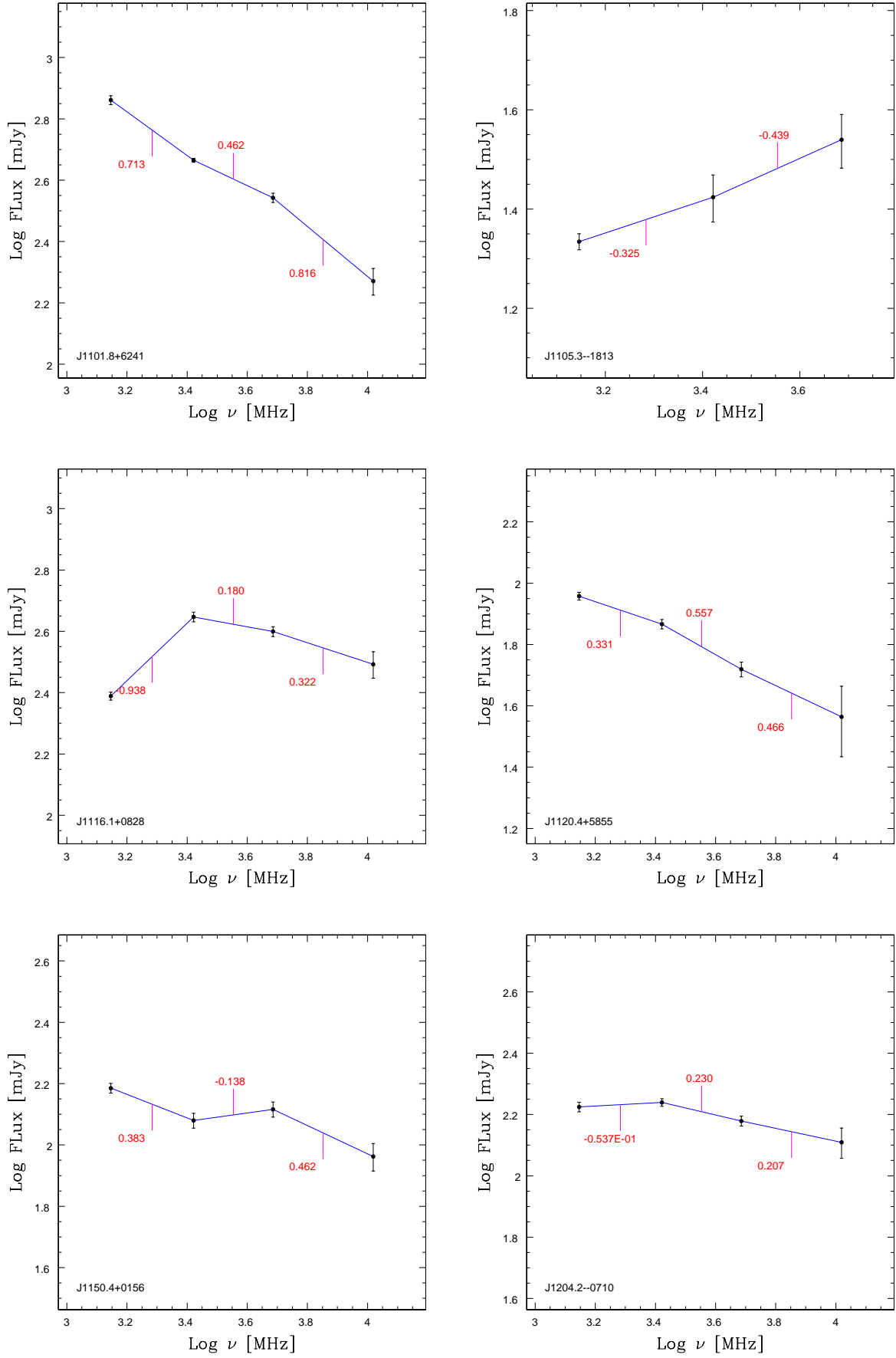


Fig. A.9. Spectral index plots of sources in Table 3.

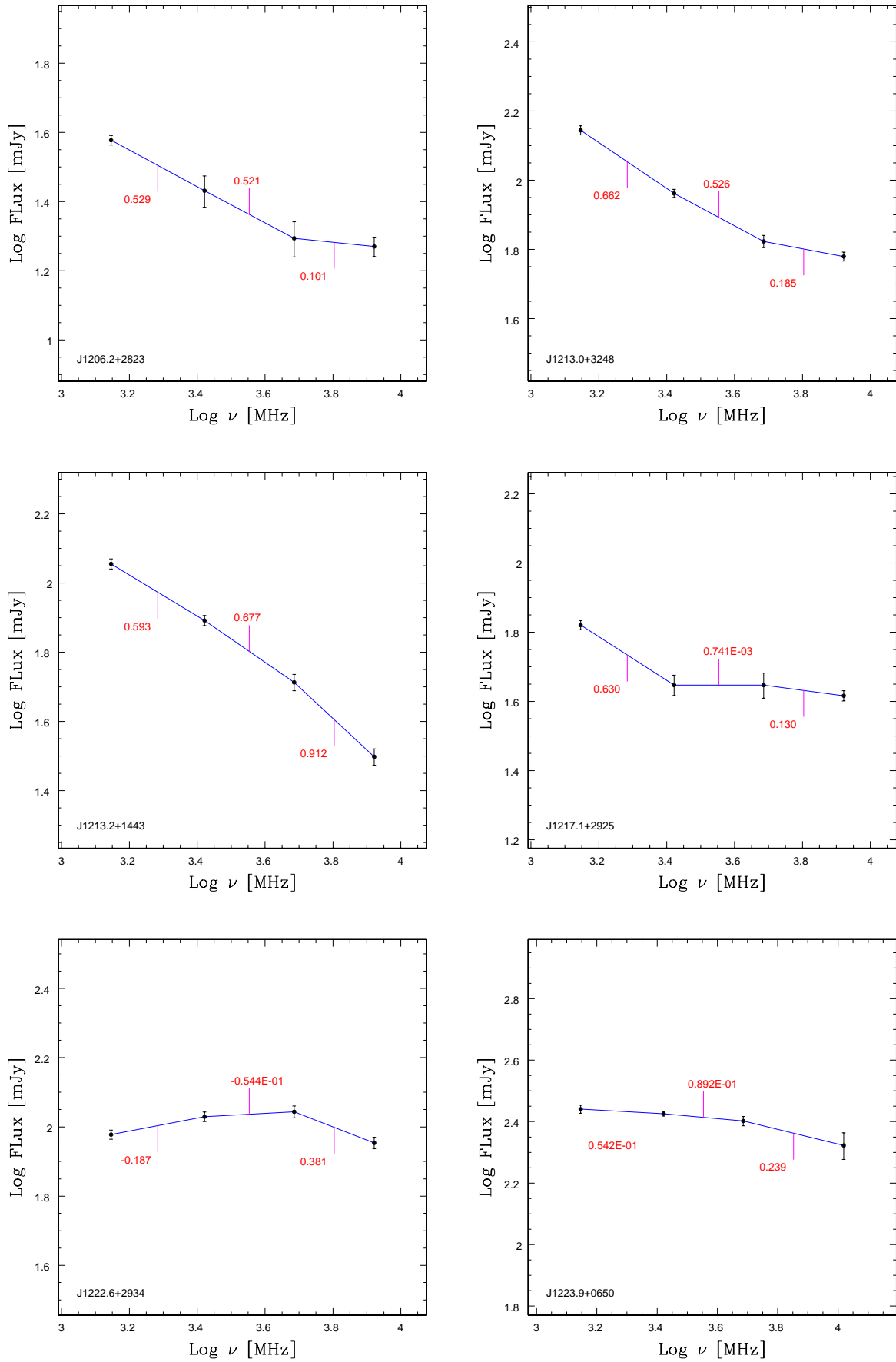


Fig. A.10. Spectral index plots of sources in Table 3.

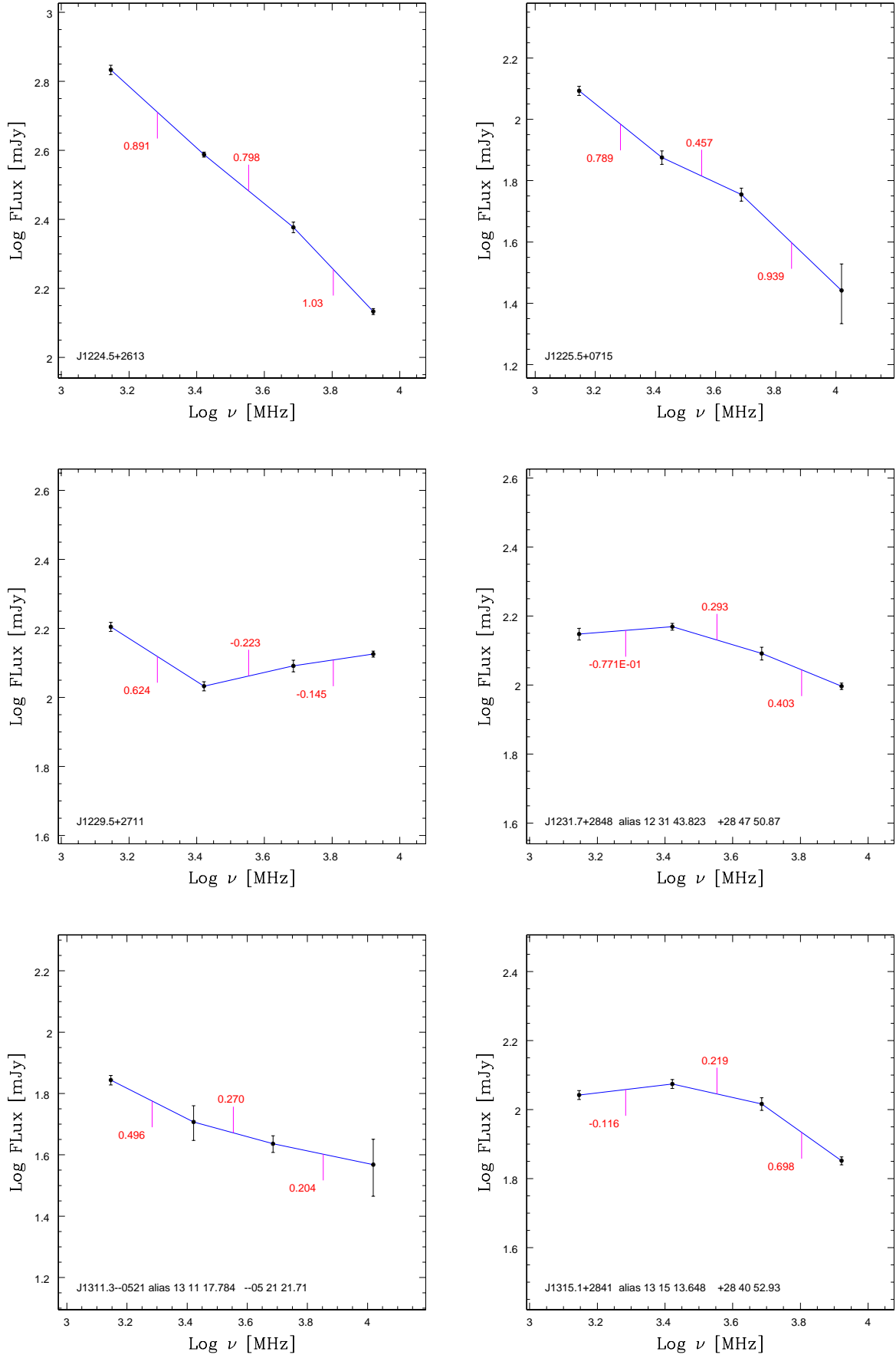


Fig. A.11. Spectral index plots of sources in Table 3.

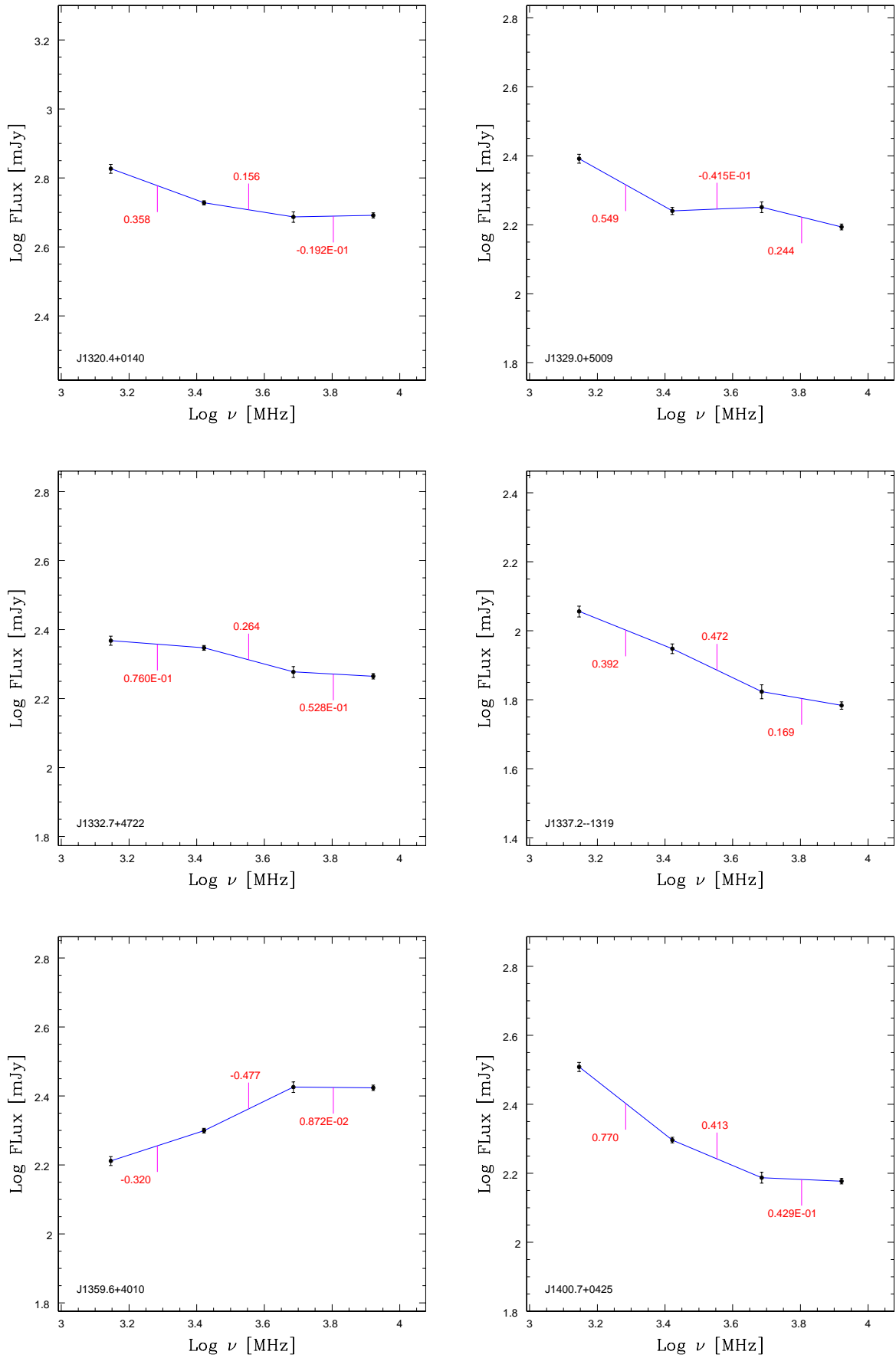


Fig. A.12. Spectral index plots of sources in Table 3.

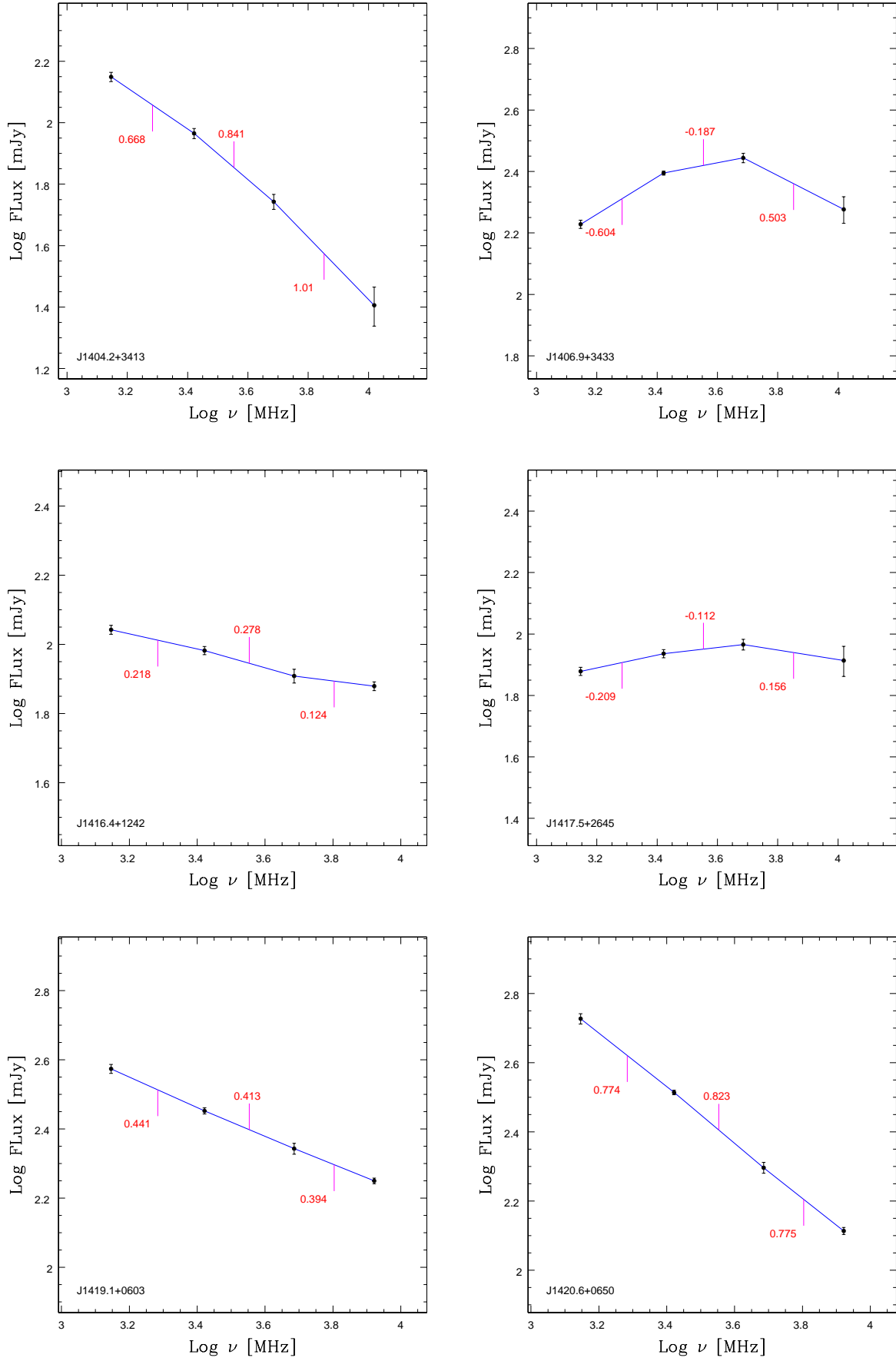


Fig. A.13. Spectral index plots of sources in Table 3.

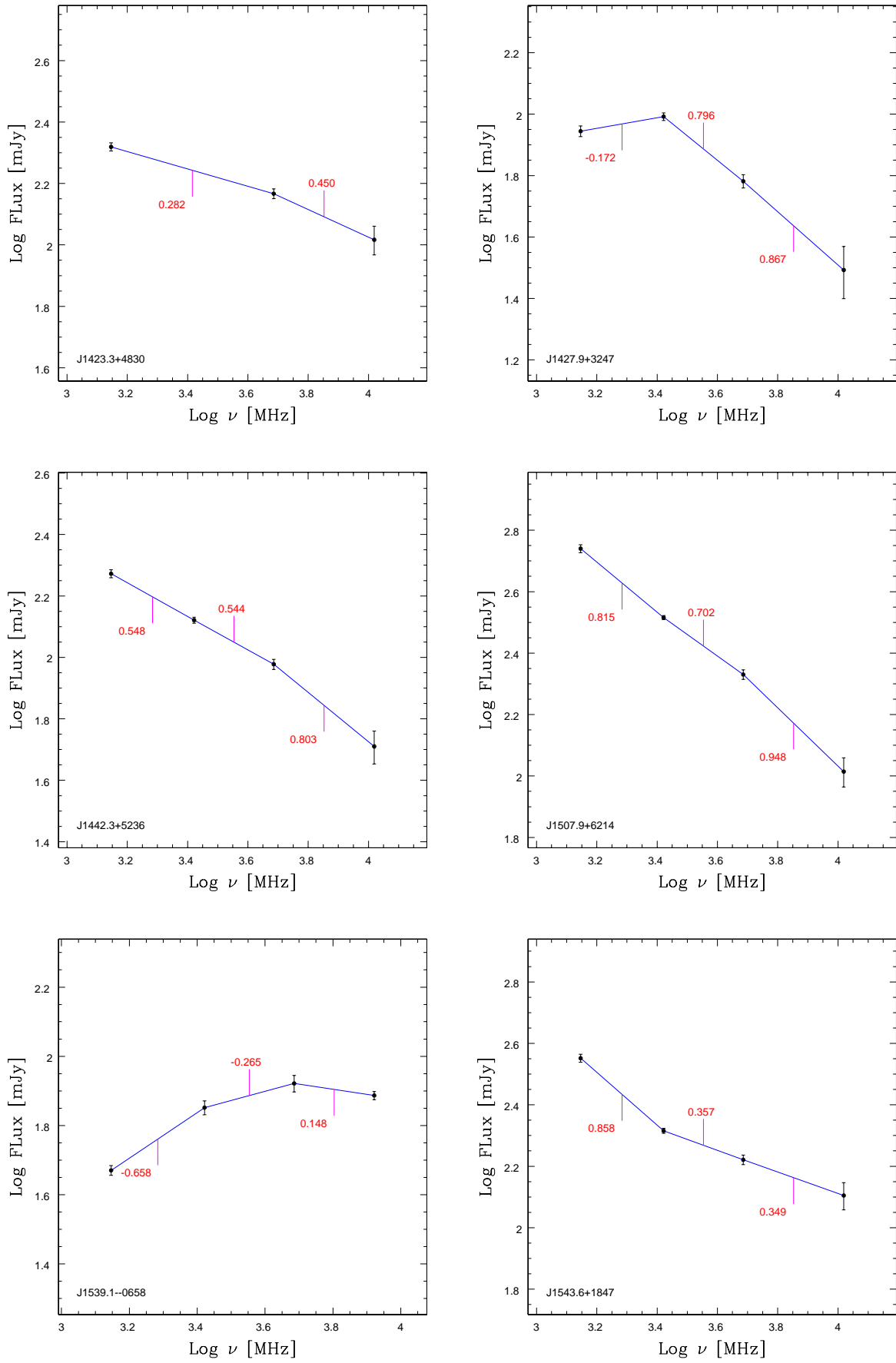


Fig. A.14. Spectral index plots of sources in Table 3.

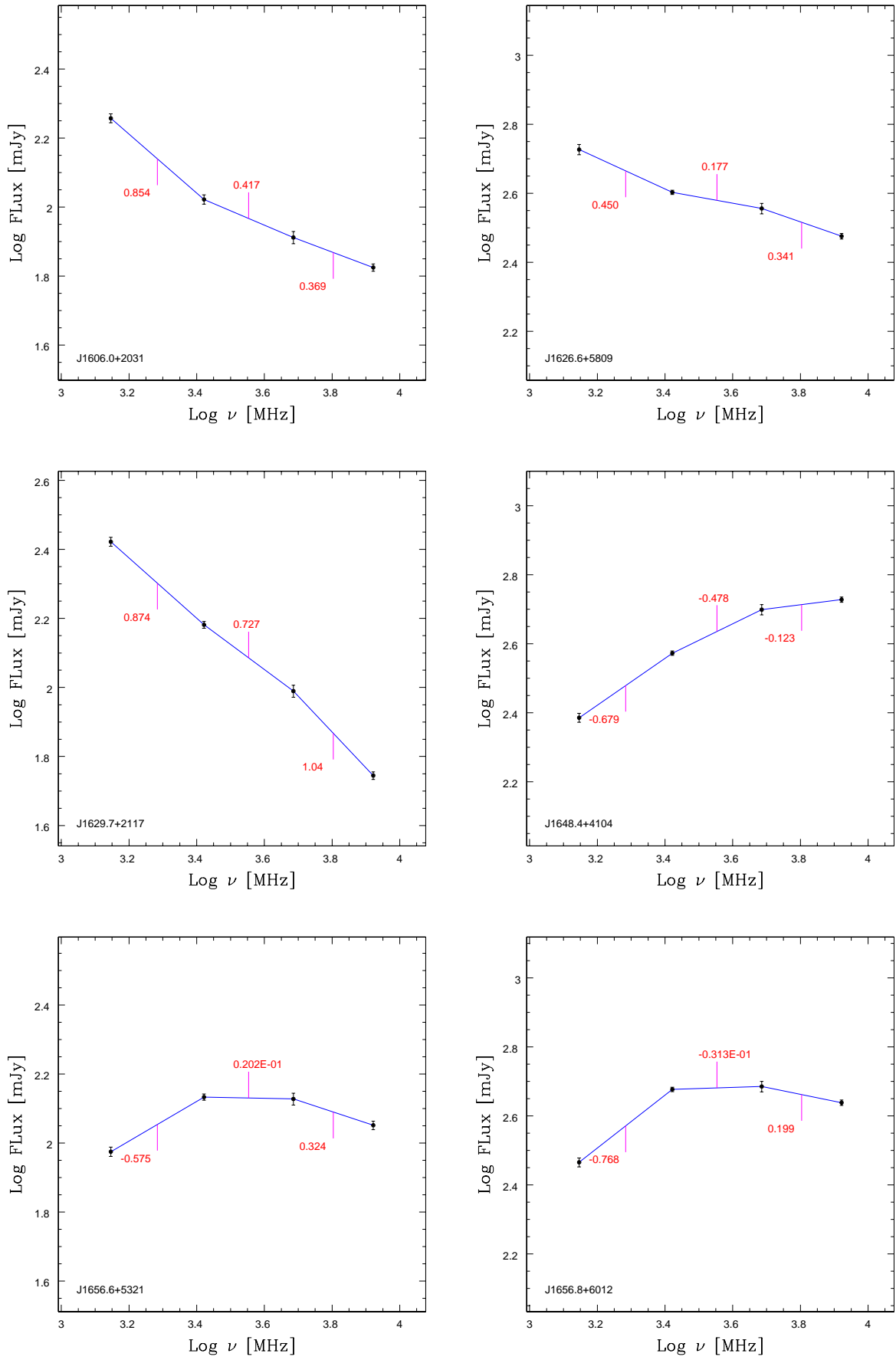


Fig. A.15. Spectral index plots of sources in Table 3.

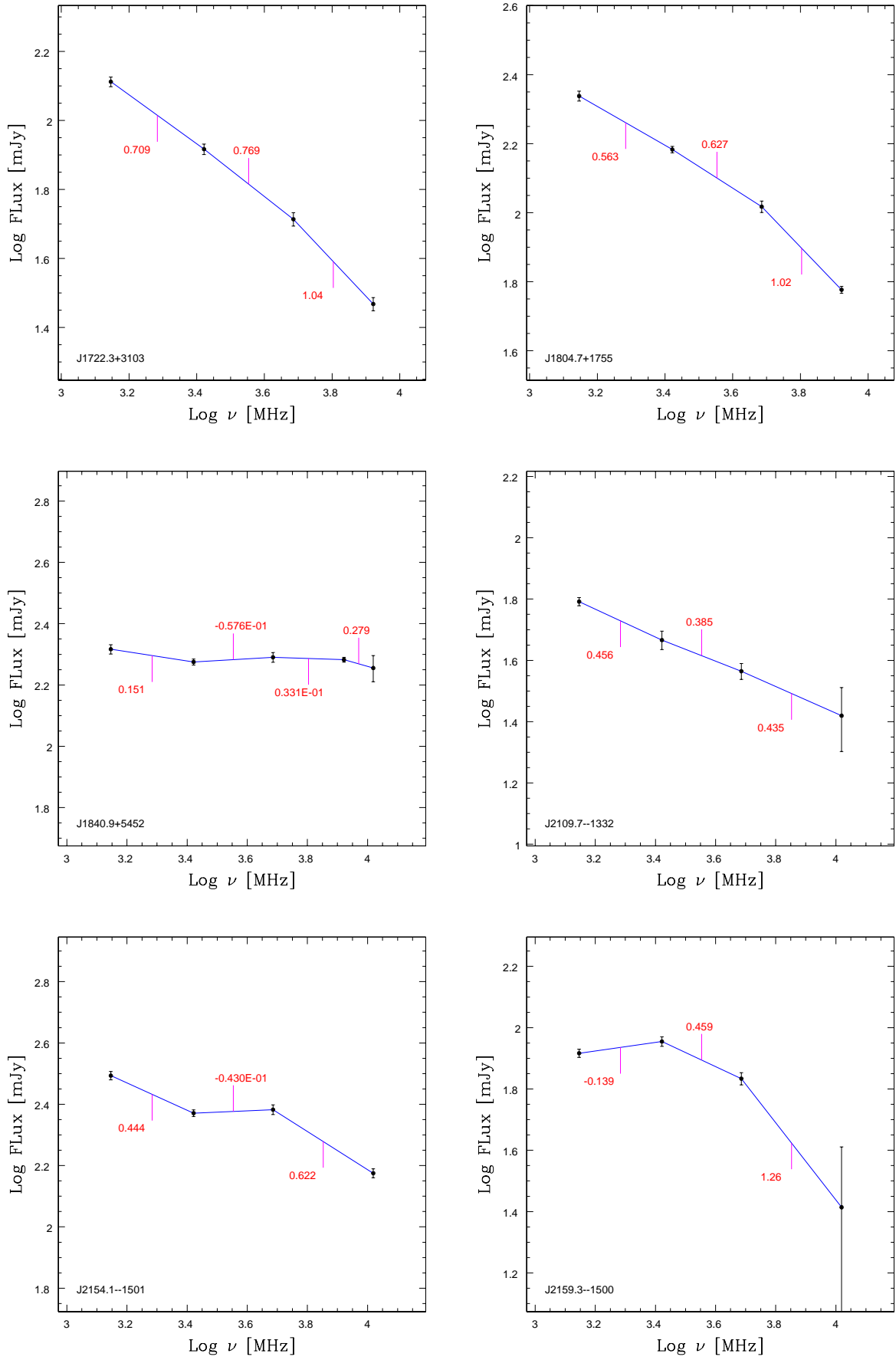


Fig. A.16. Spectral index plots of sources in Table 3.

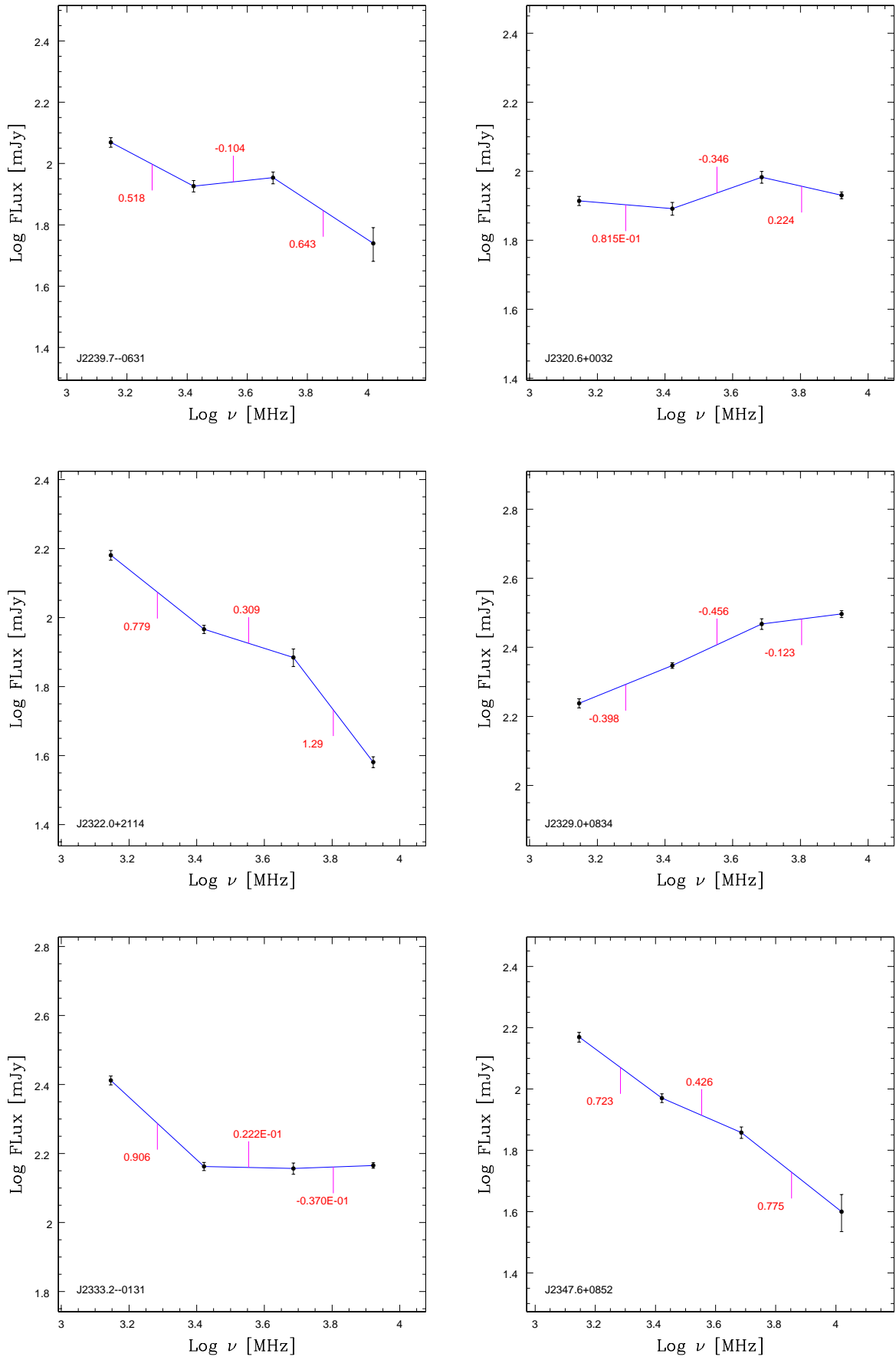


Fig. A.17. Spectral index plots of sources in Table 3.

Appendix B: RM and m plots

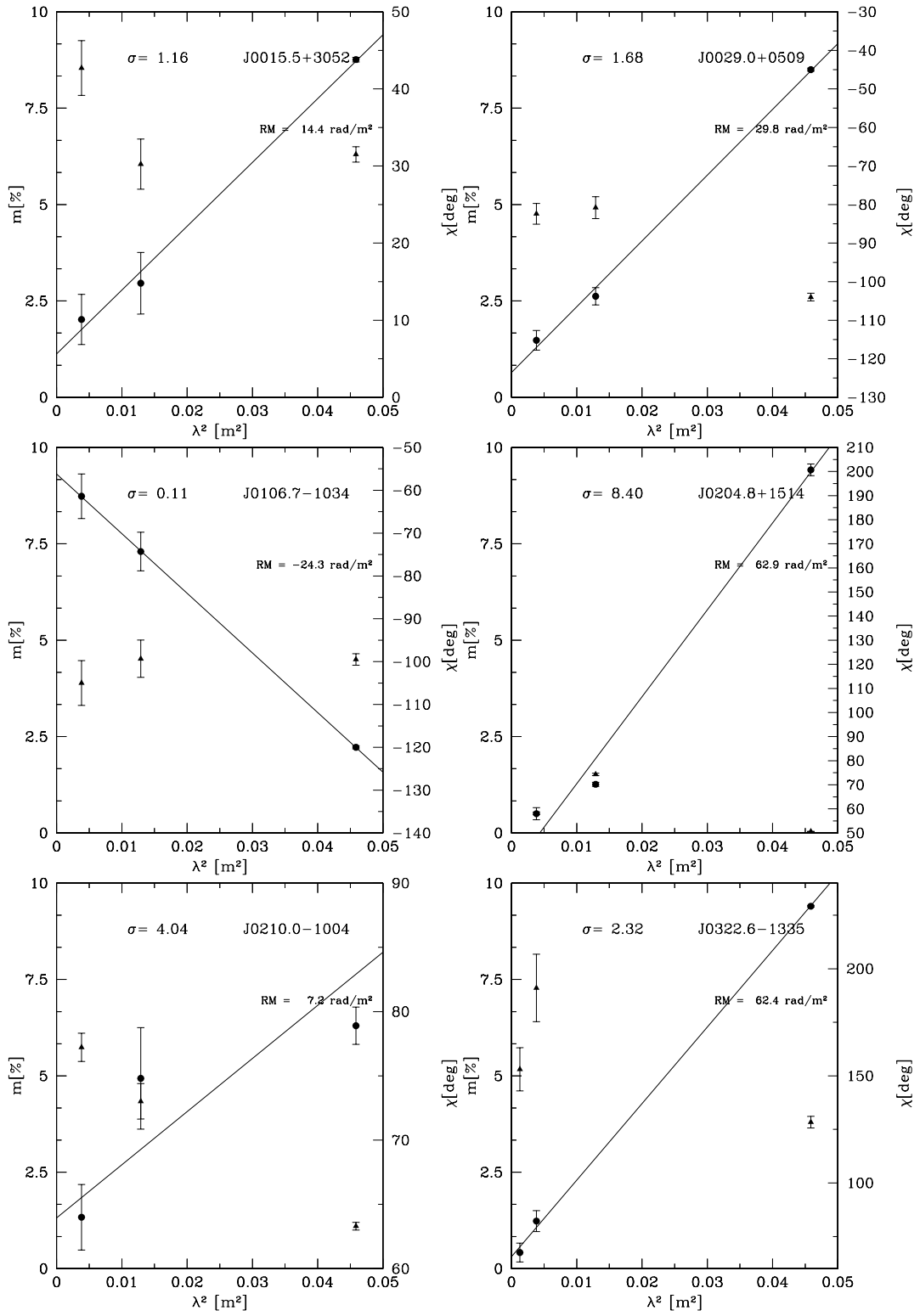


Fig. B.1. Position angles of the electric vector χ (dots) and fractional polarisation m (triangles) versus λ^2 plots of sources in Table 4. σ values assess the quality of the best fit.

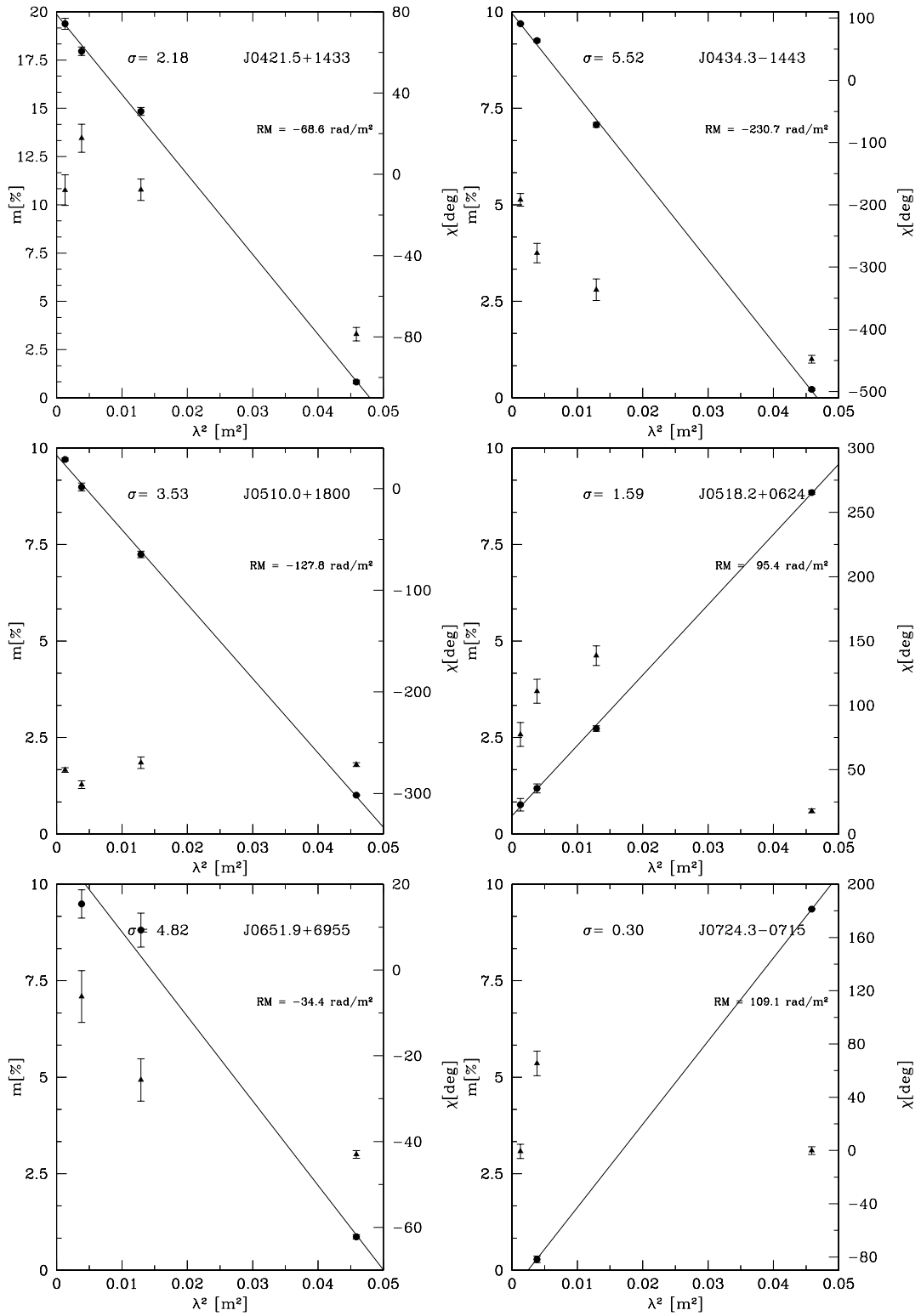


Fig. B.2. Position angles of the electric vector χ (dots) and fractional polarisation m (triangles) versus λ^2 plots of sources in Table 4. σ values assess the quality of the best fit.

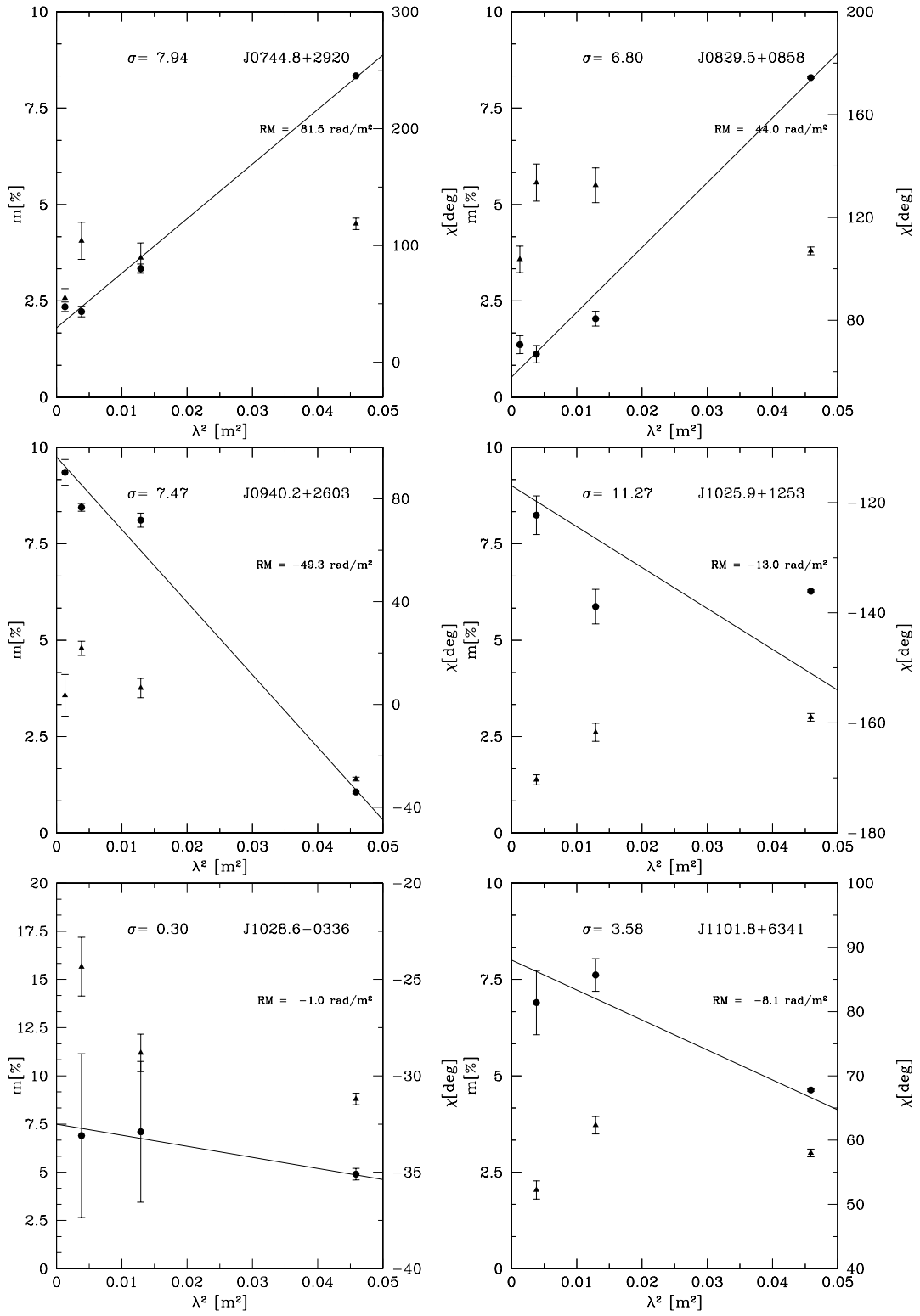


Fig. B.3. Position angles of the electric vector χ (dots) and fractional polarisation m (triangles) versus λ^2 plots of sources in Table 4. σ values assess the quality of the best fit.

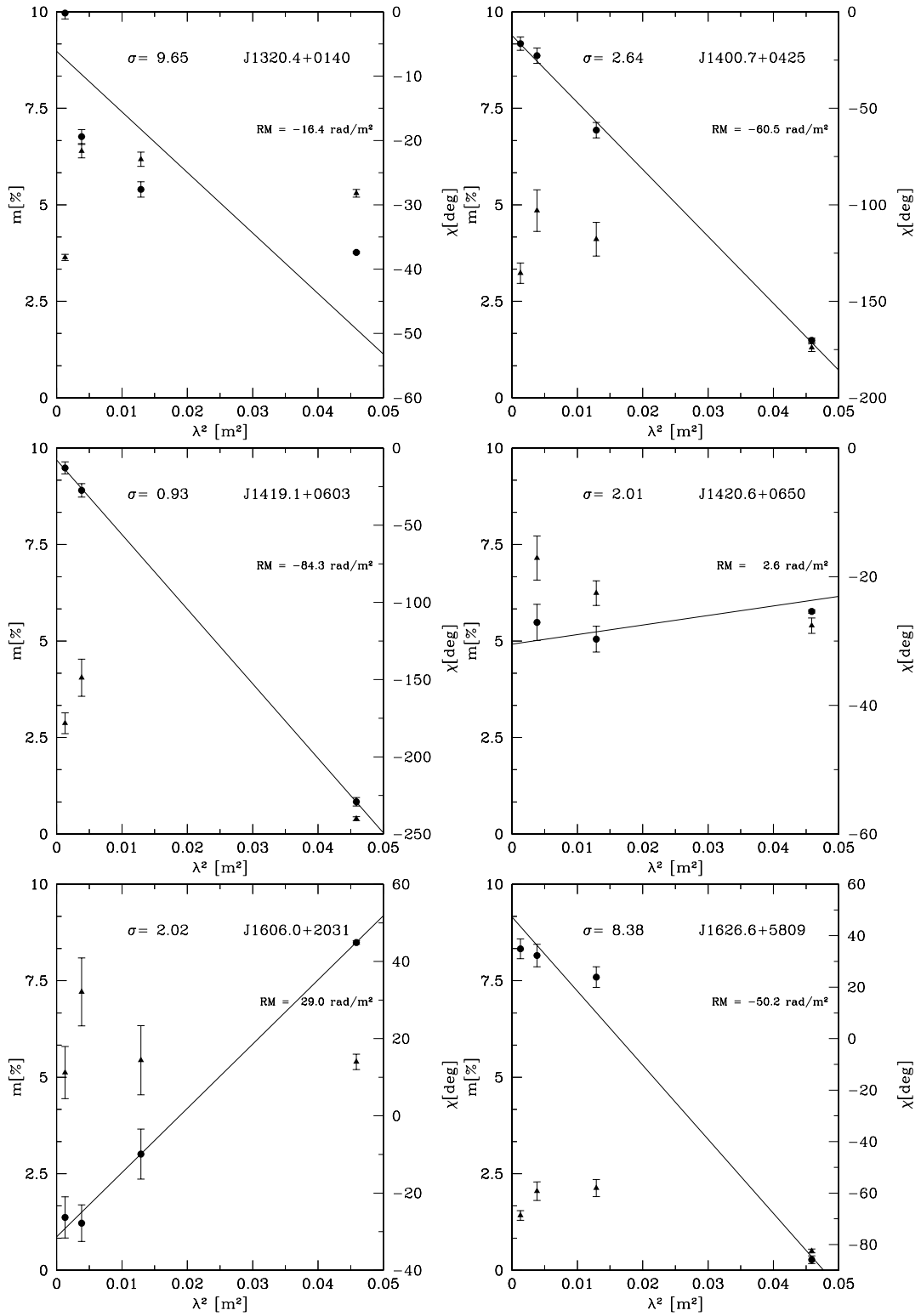


Fig. B.4. Position angles of the electric vector χ (dots) and fractional polarisation m (triangles) versus λ^2 plots of sources in Table 4. σ values assess the quality of the best fit.

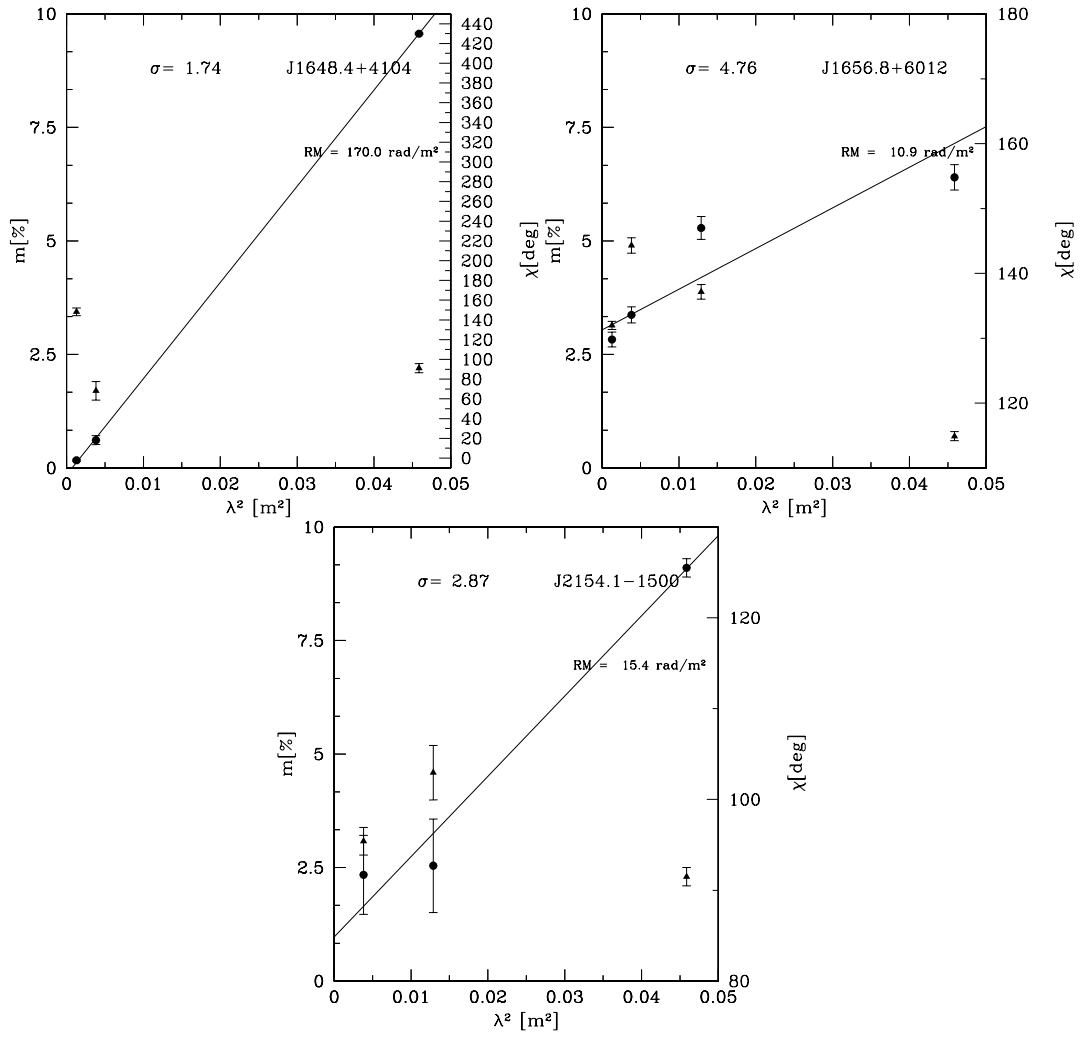


Fig. B.5. Position angles of the electric vector χ (dots) and fractional polarisation m (triangles) versus λ^2 plots of sources in Table 4. σ values assess the quality of the best fit.